Cell type-dependent escape of capsid inhibitors by simian immunodeficiency virus SIVcpz

Augustin Penda Twizerimana[1,§], Rachel Scheck[1,§], Daniel Becker[2], Zeli Zhang[1,*], Marianne Wammers[1], Leandro Avelar[2], Marc Pflieger[2], Dieter Häussinger[1], Thomas Kurz[2], Holger Gohlke[2,3], and Carsten Münk[1,#]

[1]Clinic for Gastroenterology, Hepatology, and Infectiology, Medical Faculty, Heinrich-Heine-University Düsseldorf, Düsseldorf, Germany. [2]Institute for Pharmaceutical and Medicinal Chemistry, Heinrich Heine University Düsseldorf, Düsseldorf, Germany. [3]John von Neumann Institute for Computing (NIC), Jülich Supercomputing Centre & Institute of Biological Information Processing (IBI-7: Structural Biochemistry), Forschungszentrum Jülich GmbH, Jülich, Germany.

[§] A.P.T. and R.S. made equal contribution to the execution and analysis of experiments. Author order was determined by additional contribution to drafting of the manuscript by A.P.T.

[*]Present address: La Jolla Institute for Immunology, La Jolla, CA 92037, USA

[#]Address correspondence to Carsten Münk, carsten.muenk@med.uni-duesseldorf.de

Running Title: SIVcpz escapes capsid inhibitors

ABSTRACT

Pandemic HIV-1 is the result of zoonotic transmission of *Simian immunodeficiency virus* (SIV) from chimpanzee species *Pan troglodytes troglodytes* (SIVcpzPtt). The related *Pan troglodytes schweinfurthii* is the host of a similar virus, SIVcpzPts, which did not spread to humans.

We tested these viruses with small-molecule capsid inhibitors (PF57, PF74, and GS-CA1) that interact with a binding groove in the capsid that is also used by CPSF6. While HIV-1 was sensitive to capsid inhibitors in cell lines, human macrophages and PBMCs, SIVcpzPtt was resistant in rhesus FRhL-2 cells and human PBMCs but was sensitive to PF74 in human HOS and HeLa cells. SIVcpzPts was insensitive to PF74 in FRhL-2 cells, HeLa cells, PBMCs, and macrophages, but was inhibited by PF74 in HOS cells. The truncated version of CPSF6 (CPSF6-358) inhibited SIVcpzPtt and HIV-1 while, in contrast, SIVcpzPts was resistant to CPSF6-358. Homology modelling of HIV-1, SIVcpzPtt, and SIVcpzPts capsids and binding energy estimates suggest that these three viruses bind similarly with the host proteins cyclophilin A (CYPA) and CPSF6 as well as the capsid inhibitor PF74. Cyclosporin A treatment, mutating the CYPA-binding loop in the capsid or CYPA-knockout eliminated SIVcpzPts' resistance to PF74 in HeLa cells. These experiments revealed that the antiviral capacity of PF74 is controlled by CYPA in a virus- and cell type-specific manner. Our data indicate that SIVcpz viruses can use infection pathways that escape the antiviral activity of PF74. We further suggest that the antiviral activity of PF74 capsid inhibitors depends on cellular cofactors.

IMPORTANCE

HIV-1 originated from SIVcpzPtt, but not from the related SIVcpzPts, and thus it is important to describe the molecular infection of SIVcpzPts in human cells to understand zoonosis of SIVs. Pharmacological HIV-1 capsid inhibitors (*e.g.*, PF74) bind a capsid groove that is also a binding site for the cellular protein CPSF6. SIVcpzPts was resistant to PF74 in HeLa cells but sensitive in HOS, thus indicating cell-line specific resistance. Both SIVcpz viruses showed a resistance to PF74 in human PBMCs. Modulating the presence of cyclophilin A or its binding to capsid in HeLa cells overcame SIVcpzPts resistance to PF74. These results indicate that early cytoplasmic infection events of SIVcpzPts may differ between cell types and affect, in an unknown manner, the antiviral activity of capsid inhibitors. Thus, capsid inhibitors depend on the activity or interaction of currently uncharacterized cellular factors.

INTRODUCTION

After receptor interaction, *Human immunodeficiency virus type 1* (HIV-1) infects cells by membrane fusion followed by reverse transcription of its viral genomic RNA into double-stranded DNA, which integrates into the host's chromosomal DNA in the nucleus. The capsid (CA) protein builds a cone-shaped core that delivers viral RNAs and enzymes into the cell. This core undergoes structural changes in a poorly described process called uncoating that takes place either in the cytoplasm, at the nuclear pore, or in the nucleus (1-7), where the CA protein interacts with diverse cellular proteins. To inhibit early capsid-dependent steps in viral infection, small compounds have been developed that target the CA protein (8, 9). Prominent examples of cellular human capsid interactors include cyclophilin A (CYPA, PPIA, peptidylprolyl isomerase A), TRIM5α (splice variant α tripartite motif-containing protein 5), MX2 (MX dynamin-like GTPase 2), karyopherin TNPO3 (transportin 3), CPSF6 (cleavage and polyadenylation specificity factor 6), nuclear pore proteins NUP358 (nucleoporin 358, also called RANBP2, RAN binding protein 2), and NUP153 (nucleoporin 153) (10-17). NUP153, NUP358, CPSF6, and TNPO3 promote HIV-1 nuclear entry and positively influence integration (1, 17-19). Distantly related simian immunodeficiency viruses (SIV) from African green monkeys (SIVagm) or rhesus macaques (SIVmac) also bind to NUP153 (19). Thus, it is likely that all primate lentiviruses use a similar nuclear entry pathway, but NUP153 may not be required for all SIVs (20). HIV-1 is sensitive to human TRIM5α and MX2, as well as to the experimentally expressed truncated CPSF6 (CPSF6-358) (13, 14, 17, 21-23). TNPO3 protects HIV-1 infection from CPSF6-mediated capsid stabilization in the host cell cytoplasm and prevents CPSF6 from accumulating in the cytoplasm. Mislocalization of CPSF6 to the cytoplasm, as in the case of the truncated CPSF6-358, results in the inhibition of HIV-1 (24). The oligomeric CPSF6-358 binds and disrupts the core of HIV-1 (25). Mutations in the CA

protein can generate HIV-1 variants that are resistant to these restriction factors (17, 23, 24, 26-28).

One of the best-characterized CA inhibitors is PF74 (also called PF-3450074), which binds to CA at the N-terminal domain–C-terminal domain interface between two monomers of the CA hexamer in a pocket that overlaps with the CPSF6 interface and is close to the NUP153 binding site (8, 19, 29-31). Treatment of cells with PF74 blocks HIV-1 via cooperative mechanisms of binding to the capsid and perturbs uncoating and reverse transcription at higher concentrations (5 to 10 μM); lower concentrations (up to 2 μM) block HIV-1 after reverse transcription and before nuclear entry but also reduce post-nuclear entry steps (8, 29, 32-35). Capsid inhibitors with a similar binding location are in development for clinical use (36-38).

Pandemic HIV-1 is the result of zoonotic transmission of *Simian immunodeficiency virus* from chimpanzee species *Pan troglodytes troglodytes* (SIVcpzPtt). The related chimpanzee species *Pan troglodytes schweinfurthii* is the host of a similar virus, SIVcpzPts, which did not successfully spread to humans (39-41). Like HIV-1, SIVcpzPtt is sensitive to human TRIM5α and MX2 but evolved in humans to counteract restriction by human BST2 (TETHERIN) and APOBEC3H (39, 42-45). In this study, we compared the sensitivity of HIV-1 and SIVcpz viruses to early cytoplasmic interactors, such as CYPA, CPSF6-358 and capsid inhibitors.

RESULTS

Human cell lines are differentially permissive to SIVcpz viruses. We hypothesized that the human-adapted HIV-1 and the chimpanzee-adapted SIVcpz viruses differ in their capacity to interact with cytoplasmic cellular factors. We decided to study capsid interacting proteins CYPA, CPSF6-358 and capsid inhibitors binding in the CPSF6-groove of capsid. To identify suitable cell-systems for our experiments, we tested commonly used cell lines with SIVcpzPtt, SIVcpzPts and HIV-1, VSV-G pseudotyped luciferase reporter viruses. We infected two human cell lines (HeLa and HOS), three simian cell lines (CV-1 from African green monkeys, FRhL-2 from rhesus macaques, and OMK from owl monkeys), and one feline cell line (CRFK) and measured luciferase activity two days post-infection. Feline cells do not express a restricting TRIM5α protein (46), while CV-1, FRhL-2 express TRIM5α proteins, and OMK express TRIM5Cyp that inhibit HIV-1 (47). Titration infection experiments confirmed that both human cell lines were equally permissive to HIV-1, while CRFK cells were 10-fold more susceptible than HeLa or HOS, and that HIV-1 was restricted in simian cells (48-50) (Fig. 1A). The difference in infectivity between the permissive CRFK and the restrictive OMK cells was up to 10,000-fold. HIV-1 was slightly more restricted in OMK than in CV-1 cells, but both SIVcpzPtt and SIVcpzPts were equally inhibited in these simian cells (Fig. 1B, 1C). In further contrast to HIV-1, human HOS cells were more or equally permissive compared with CRFK cells to SIVcpzPtt and SIVcpzPts. For HIV-1 infections, the HOS and HeLa cells displayed comparable permissiveness; however, HeLa cells were 33- and 20-fold less infectable by SIVcpzPtt and SIVcpzPts, respectively, than HOS cells. Infection by HIV-1, SIVcptPtt, and SIVcpzPts was lower in FRhL-2 cells than in HeLa cells and the differences were greatest with HIV-1 (Fig. 1D, 1E, and 1F). We analyzed the presence of important host proteins in HOS and HeLa cells by immunoblots and found that the two cell lines express similar amounts of

TRIM5α, CYPA, CPSF6, NUP153, and NUP358 (Fig. 1G). Thus, the expression levels of these proteins cannot explain the different sensitivities of HOS and HeLa cells to the two SIVcpz viruses.

SIVcpz viruses show cell-type-specific sensitivity to Cyclosporin A. Cyclophilin A is a cellular protein that has several postulated functions in HIV-1 infection (18, 32, 51-61). CYPA interacts with the capsid of HIV-1 (62) and is incorporated into nascent viral particles (10, 11). In the HIV-1 capsid, CYPA targets a proline-rich loop (also called CYPA-binding loop) with key interacting residues G89 and P90 (63). Cyclosporin A (CsA) is a natural product from a fungus that binds to CYPA and other cyclophilins and CsA treatment of cells disrupts CYPA incorporation into budding HIV-1 virions (62, 64). HIV-1 mutation of the CYPA-binding loop, depletion of CYPA in cells, or inhibition by the use of CsA were instrumental in identifying cell types in which HIV-1 depends on CYPA such as HOS and primary CD4+ T cells, and cell types in which HIV-1 replicates independently of CYPA such as HeLa cells (56, 61, 65-71). We aligned the capsid residues of HIV-1 and SIVcpz viruses that are involved in the interaction with CYPA, CPSF6, and capsid inhibitors (Fig. 2A and 2B; Fig. S1 and S2). Despite similarities in capsid G89 and P90, which are residues known to be important for the interaction between HIV-1 capsid and CYPA, the alignment highlights differences in the CYPA-binding loop on the capsids of HIV-1 and SIVcpz viruses (Fig. 2A and 2B). Most residues are highly or absolutely conserved within HIV-1 and SIVcpz sequences, respectively, which predominantly also applies to residues interacting with a ligand (marked by stars in Fig. 2A and 2B). Only residues 91-93 that interact with CYPA (blue stars in Fig. 2A and 2B) show a higher sequence variability containing also non-conservative substitutions within one lineage as well as between lineages. Binding mode models of human CYPA to HIV-1, SIVcpzPts, and SIVcpzPtt

CA proteins confirmed that the interacting residues differ in three positions between HIV-1 CA and SIVcpzPts CA: ILE91 vs. GLN91; ALA92 vs. GLN92; PRO93 vs. ALA93. The interacting residues differ in one position between HIV-1 CA and SIVcpzPtt CA (ALA92 vs. PRO92) (Fig. 3A and 3B).

To identify whether viral particles of SIVcpz and HIV-1 package CYPA in a similar manner, immunoblots of virions were analyzed. In virions of SIVcpzPtt and SIVcpzPts levels of CYPA were similar to HIV-1 particles, and treatment of virus-producing cells by CsA blocked CYPA packaging by all three viruses (Fig. 4A). Glutathione S-transferase (GST)-pulldown experiments were performed to test the binding of CYPA to SIVcpz GAG. HEK293T cells were co-transfected with plasmids for SIVcpz or HIV-1 and CYPA-GST in the presence or absence of CsA. Following transfection, cells and viruses were lysed and the lysates were used for pulldown experiments using GST-sepharose beads. Immunoblotting of the precipitated complexes demonstrated that CYPA-GST interacted with GAG of HIV-1, SIVcpzPtt, and SIVcpzPts (Fig. 4B). Importantly, GST alone did not precipitate GAG and the administration of 10 µM CsA prevented the binding of CYPA to GAG equally for all three viruses, in contrast, viruses carrying the G89V mutation in the presumed CYPA binding loop of the capsid (Fig. 2A) did not bind CYPA (Fig. 4C).

Since the activity of CYPA in the HIV-1 target cells, and not the virus-producing cells, regulates HIV-1 replication (56, 68), we treated human HOS and HeLa and rhesus macaque FRhL-2 cells with increasing amounts of CsA before infection. Cyclosporin A treatment made HOS cells up to 6-fold more resistant to HIV-1 but increased the infection in HeLa and FRhL-2

177 cells (Fig. 5A). Infections with both SIVcpz viruses demonstrated that CsA treatment of either
178 cell line had no inhibitory consequences and, in fact, stimulated infection (Fig. 5B and 5C).
179 However, in HOS cells, CsA did not enhance SIVcpzPtt infection (Fig. 5B). To determine
180 whether these observations were related to the CYPA protein, we tried to generate HOS and
181 HeLa *CYPA* knockout (KO) cells (Fig. 6A and 6B). In HOS cells, the population of cells showed
182 only a weak loss of CYPA protein in immunoblots and thus, we established and used clonal
183 cell lines that had a large deficiency in CYPA (Fig. 6A). HOS CYPA KO clones 1, 3, and 5
184 showed reduced susceptibility to HIV-1 and SIVcpzPtt but not to SIVcpzPts (Fig. 6C - E).
185 Treatment of the HOS.CYPA KO cells with 5 µM CsA at infection did not significantly further
186 increase the restriction of HIV-1, but, surprisingly, reverted the inhibition of SIVcpzPtt (Fig.
187 6D) and enhanced the infections by SIVcpzPts of WT HOS cells and of HOS.CYPA KO cells (Fig.
188 6E). In HeLa cells we found a significant knockdown (KD) of CYPA in the population of cells
189 and these HeLa.CYPA KD cells were used for infections (Fig. 6B). CYPA-deficient HeLa cells
190 showed a mild increase in permissiveness to HIV-1 (less than 2-fold, Fig. 6F) and were 5-to 6-
191 fold more permissive to SIVcpzPtt and SIVcpzPts (Fig. 6G, 6H). To test the effect of CsA on
192 the infection of these viruses in CYPA-deficient HeLa cells, cells were pre-treated with 5 µM
193 CsA and infected. Experiments in WT HeLa cells in the presence of CsA revealed similar data
194 to that shown in Fig.5 and infection of SIVcpzPtt and SIVcpzPts was more enhanced than the
195 infection of HIV-1 (Fig. 6F - H). Interestingly, HIV-1 infection was not increased by CsA
196 treatment in HeLa.CYPA KD cells and its infectivity was reduced by 30% (Fig. 6F). On the
197 other hand, in HeLa.CYPA KD cells, SIVcpzPtt and SIVcpzPts viruses infected 5- and 2-fold
198 more in the presence of CsA, respectively (Fig. 6G, 6H). Remarkably, the combination of
199 CYPA deficiency and CsA treatment enhanced the permissiveness of HeLa cells 30- and 11-
200 fold to SIVcpzPtt and SIVcpzPts, respectively. Taken together, these data indicate that CYPA

is involved in SIVcpzPtt and SIVcpzPts infection and, for SIVcpzPts, blocking or removing CYPA enhances infection in human HOS and HeLa cells, while SIVcpzPtt enhancement is only seen in HeLa cells. Our data also suggest that CsA treatment influences CYPA-independent pathways of SIVcpz infection.

SIVcpzPts is insensitive to CPSF6-358. To test the effect of CPSF6-358, we generated HOS cells that expressed CPSF6-358 (HOS.CPSF6-358, Fig. 7A). In HOS.CPSF6-358 cells, infection of HIV-1 was reduced compared to HOS cells with the empty vector, while HIV-1 with CA mutants in the CPSF6-binding site (N74D or A77V, Fig. 2A (72)) escaped this restriction (Fig. 7B, 7C, and 7D). CPSF6-358 also inhibited HIV-1 in HOS.CYPA KO cells (Fig. 7B). SIVcpzPtt showed a pattern of restriction in these cell lines similar to that of WT HIV-1 (Fig. 7E). In contrast, CPSF6-358 did not inhibit SIVcpzPts in WT HOS or HOS.CYPA KO cells (Fig. 7F).

Although no crystal structure information of a CPSF6/SIVcpz CA complex is available, CPSF6 likely binds at the same site in SIVcpzPts or SIVcpzPtt CA like in HIV-1 CA because of the high sequence identity between the proteins (HIV-1 CA vs. SIVcpzPts CA: 79%; HIV-1 CA vs. SIVcpzPtt CA: 90%; Fig. 2A and 2B). The binding sites are located in the interface between two monomers, which are part of the hexameric CA structure. Although the binding sites for CPSF6 are highly similar for HIV-1 CA vs. SIVcpzPtt CA (identity of 24 residues involved in CPSF6 binding: 96%), the HIV-1 CA vs. SIVcpzPts CA binding sites are more distinct (88%) (Fig. 8A and 8B). To gain further insights, we generated structural models of CPFS6/CA proteins, using in all cases homology models of the CA proteins to improve their comparability. All

223 homology models are of high structural quality, as indicated by the model quality
224 assessment program TopScore (73) (Fig. 2C, 2E).

225 The binding site of SIVcpzPtt differs in one residue to HIV-1: SER178' vs. THR178' (Fig. 8A -E).
226 As in this case the closest residue of CPFS6, GLN319, interacts with its N_{δ} with the backbone
227 O of either serine or threonine, no impact of this substitution on CPSF6 binding is expected.

228 The binding site of SIVcpzPts CA differs in three residues to HIV-1 CA: SER102 vs. ALA102;
229 LEU172' vs. ILE175'; ASN183' vs. THR186' (dashed residue names indicate a residue location
230 on the second monomer; Fig. 8A -E). As residue 102 is more than 4.4 Å away from CPSF6, no
231 direct impact on CPSF6 binding due to this substitution is expected. Residue 102 differs also
232 within SIVcpz viruses: ALA102 and SER102 appear equally frequent in all investigated SIVcpz
233 sequences (Fig. 2B). The substitution of leucine by isoleucine is a conservative one both with
234 respect to the size of the residue and the potential interactions with CPSF6 and, hence, is not
235 expected to influence CPSF6 binding either. Yet, the substitution of asparagine by threonine
236 may have an impact. Besides the difference in the size of the residues, C_{γ} of threonine and
237 the phenyl ring of PHE316 of CPSF6 form a close contact that is not present in the case of
238 asparagine. To conclude, the structural analysis of binding mode models of CPSF6 in all three
239 CA proteins suggests that CPSF6 binding to HIV-1 CA and SIVcpzPtt CA is similar, whereas
240 differential binding may be expected in the case of SIVcpzPts CA. These results parallel the
241 above ones on the sensitivity of HIV-1 or SIV infections in the presence of CPSF6-358.

242

243 **SIVcpz viruses, but not HIV-1, show cell-type-specific sensitivity to capsid inhibitors.** The
244 unexpected observation that the non-zoonotically transmitted SIVcpzPts was insensitive to
245 CYPA KO or expression of CPSF6-358 in HOS cells motivated us to test capsid inhibitors that

246 bind in the same capsid pocket as CPSF6 (Fig. 9A). We tested three cell lines (human HOS
247 and HeLa, and rhesus macaque FRhL-2) and compared the strong inhibitor PF74 with the
248 less-potent variant PF57 (PF-3759857 (8)) from 0.5 µM to 8 µM. HIV-1 was inhibited in all
249 three cell lines by both inhibitors in a dose-dependent manner up to 100-fold by PF74 and
250 up to 10-fold by PF57 (Fig. 9B, 9C). Each cell line showed a slightly different dose-response
251 curve, and the inhibitory effect of both inhibitors was strongest in FRhL-2 cells. Infection by
252 SIVcpzPtt and SIVcpzPts was different compared to that by HIV-1. PF57 and PF74 inhibited
253 both SIVcpz viruses in human HOS cells in a dose-dependent manner to levels that were
254 comparable to the inhibition of HIV-1 (Fig. 9D – G). PF74 reached a saturating inhibition at
255 the lowest tested concentration for SIVcpzPtt in HeLa cells and this inhibition was 10-fold
256 less than that in HOS cells (Fig. 9D). PF57 at 8 µM restricted SIVcpzPtt in HeLa cells similar to
257 that in HOS cells, but the dose-response curves differed (Fig. 9E). Neither inhibitor exhibited
258 antiviral activity against SIVcpzPtt in the rhesus macaque FRhL-2 cell line (Fig. 9D, 9E). More
259 unexpected results were obtained when testing SIVcpzPts. This virus was only sensitive to
260 capsid inhibitors in human HOS cells but showed resistance in human HeLa and simian FRhL-
261 2 cells (Fig. 9F, 9G). To rule out an effect of TRIM5α, which may be a factor that regulates
262 viral susceptibility to capsid inhibitors, we infected feline CRFK cells that naturally lack the
263 expression of a restricting TRIM5α protein with HIV-1 and both SIVcpz viruses (46). In CRFK
264 cells, all three viruses were sensitive to PF74 and PF57, but SIVcpzPts was the least inhibited
265 (Fig. 10A - C).

266 The recently described small-molecule HIV CA inhibitor GS-CA1 (Fig. 10D) has in comparison
267 to PF74 a >5000-fold more potent antiviral activity against HIV-1; both inhibitors use the
268 same binding groove in CA (38). Using 10 nM of GS-CA1 was sufficient to inhibit HIV-1
269 infection of HeLa cells more than 400-fold. In comparison, SIVcpzPtt was inhibited only 16-

fold and SIVcpzPts only 3-fold by this concentration of GS-CA1 in HeLa cells (Fig. 10E – G). Despite structural differences of PF74 and GS-CA1, SIVcpz viruses are 25- to 130-fold less sensitive to GS-CA1 than HIV-1.

To test if the resistance to capsid inhibitors is also seen in primary human cells, we infected macrophages and PBMCs in the presence of PF74. HIV-1 was inhibited up to 10-fold by PF74 in PMBCs and macrophages (Fig. 11A - D), while PF74 could not block the infection of SIVcpzPtt and SIVcpzPts in PBMCs (Fig. 11A, 11B). However, in macrophages, PF74 showed some activity against SIVcpzPtt (up to 2-fold inhibition), but not SIVcpzPts (Fig. 11C, 11D). Together, these results demonstrate that SIVcpz viruses in principle are sensitive to capsid inhibitors and that cellular factors may regulate whether these compounds can target these viruses.

Binding sites for PF74 are highly similar in the three CA proteins. In HIV-1 CA, the binding site for PF74 is also located in the interface between two monomers, like for CPSF6 (31) (Fig. 12A, 12B). Yet, PF74 is smaller and interacts with only 16 residues compared to CPSF6 (Fig. 2A). Although no crystal structure information of a PF74/SIVcpz CA complex is available, PF74 likely binds at the same site in SIVcpzPts or SIVcpzPtt CA like in HIV-1 CA because of the high sequence identity between the proteins (Fig. 2A). In particular, the sites for binding or putative binding of PF74 are identical for HIV-1 CA vs. SIVcpzPtt CA and highly similar for HIV-1 CA vs. SIVcpzPts CA ((identity of residues involved in PF74 binding: 94%) (Fig. 2A, 2B, 2D, 2F, 12A, 12B). The putative binding site of SIVcpzPts differs in one residue to HIV-1: LEU172’ vs. ILE175’ (Fig. 2A, 2B, 12A, 12B). As discussed above, this is a conservative

293 substitution likely with no impact on PF74 binding. To conclude, the structural analysis of
294 binding mode models of PF74 in all three CA proteins suggests that PF74 binding is highly
295 similar to the three proteins.

296

297 **Effective binding energy of PF74 is indistinguishable for HIV-1 and SIVcpzPts/Ptt CA**
298 **proteins.** To validate the structural analysis of PF74 binding to HIV-1 and SIVcpzPts/Ptt CA
299 proteins, we performed end-point free energy computations using the molecular mechanics
300 Poisson-Boltzmann (MM-PBSA) method (74) and the single trajectory approach (75) based
301 on five replica of molecular dynamics simulations for each PF74/hexameric CA protein
302 complex of 200 ns length each (Fig. 12C). In all MD simulations, PF74 remained in the initial
303 binding pose (no-fit PF74 root mean square deviations (RMSD) in general < 3 Å, except for
304 one binding site each in one replica each for SIVcpzPts (pink), and SIVcpzPtt; data not
305 shown). Furthermore, the C_α-atom RMSD of binding site residues is mostly around 1 Å (data
306 not shown). Both results indicate that the initial starting structures of PF74 in homology
307 models of CA proteins are plausible. The computed effective binding energies are generally
308 stable over the simulation times and form Gaussian-shaped cumulative distributions (Fig.
309 12C). They mutually differ by less than 1 kcal mol^{-1} for the three PF74/CA protein complexes.
310 As chemical accuracy is ~1 kcal mol^{-1}, which is the expected accuracy in an optimal case (76),
311 the values are thus indistinguishable from each other (Fig. 12C). To conclude, effective
312 binding energy computations on PF74/CA protein complexes corroborate that PF74 binding
313 is highly similar to the three proteins.

314

Cyclosporin A treatment or mutations in the CYPA binding loop rescue PF74 activity against SIVcpzPts in HeLa cells. To investigate whether CsA treatment affects the viral sensitivity to capsid inhibitors, drug combinations of CsA and PF74 were tested. We used either PF74 alone (1, 4, or 8 µM) or in combination with CsA (1 or 10 µM) in HeLa cells. Infections were normalized to cells treated with either DMSO or CsA only to measure the inhibitory capacity of PF74. In HIV-1-infected cells, the addition of 10 µM CsA enhanced the antiviral activity of PF74 2- to 10-fold, 1 µM CsA did not change the viral sensitivity to 1 µM PF74, but led to more inhibition at higher PF74 concentrations (Fig. 13A). A similar result was found in SIVcpzPtt infections, although, 1 µM of CsA slightly reduced the inhibition of 1 µM PF74 and 10 µM CsA enhanced inhibition by 8 µM PF74 by 18-fold (Fig. 13B). Interestingly, CsA treatment changed the resistance of SIVcpzPts to PF74, and both 1 µM and 10 µM CsA enhanced the antiviral activity of higher concentrations of PF74 by 14-fold (Fig. 13C). Similar results were also obtained using PF57 (data not shown).

The finding that treatment of HeLa cells with CsA reverses the PF74 resistance of SIVcpzPts motivated us to ask if the capsid binding to CYPA is important for this phenotype. For these experiments, we used viruses that carry the G89V mutation in the capsid loop that interacts with CYPA. HIV-1 G89V together with a low concentration of PF74 had 2-fold higher sensitivity, but PF74 concentrations above 1 µM inhibited HIV-1 WT and G89V equally (Fig. 13D). PF74 had 5-to10-fold increased antiviral activity against SIVcpzPtt G89V compared to WT virus (Fig. 13E). Strikingly, the mostly PF74-resistant virus, SIVcpzPts, was completely sensitive to the capsid inhibitor for up to 50-fold inhibition, when mutated to G89V in CA (Fig. 13F). Infections of HIV-1 and SIVcpz WT and G89V viruses in the presence of GS-CA1 generated similar results for HIV-1 and SIVcpzPtt, but the moderate inhibition of SIVcpzPts was only enhanced 5-fold by the G89V mutation (Fig. 13G - I). Our findings suggest that an

important regulator of the antiviral activity of PF74-like capsid inhibitors is a CsA-sensitive protein, which is likely the SIVcpz capsid-interacting CYPA.

Cyclophilin A knockout overcomes the resistance of SIVcpzPts to capsid inhibitors in HeLa cells. To test whether the presence of CYPA in the viral target cells protects SIVcpzPts against capsid inhibitors, HeLa.CYPA KD and HOS.CYPA KO cells (clone 3) were infected in the presence of increasing amounts of PF74 or PF57. In HeLa.CYPA KD cells compared to WT cells, HIV-1 was less inhibited by lower concentrations of PF74 and similarly inhibited at higher concentrations (Fig. 14A), which is similar to previously described results (33). In contrast, PF57 showed reduced activity against HIV-1 in HeLa.CYPA KD cell compared to WT cells at all drug concentrations (Fig. 14B). This pattern of inhibition was also seen in HOS.CYPA KO cells for HIV-1 (Fig. 14C and 14D), SIVcpzPtt (Fig. 14G and 14H) with PF74 and PF57 and for SIVcpzPts treated with PF57 (Fig. 14L). PF74 inhibited SIVcpzPts in HOS.CYPA KO cells compared to WT cells with reduced activity at low concentrations and higher inhibition at increased drug concentrations (Fig. 14K).

HeLa.CYPA KD cells infected with the SIVcpz viruses displayed two further inhibition curves. CYPA KD in HeLa cells minimally (less than two-fold) enhanced PF74 activity but did not change PF57 activity against SIVcpzPtt (Fig. 14E, 14F). SIVcpzPts demonstrated the expected resistance to both capsid inhibitors in WT HeLa cells, but, this resistance was completely lost in HeLa.CYPA KD cells (Fig. 14I, 14J), suggesting that in HeLa cells CYPA is an antagonist of capsid inhibitors for SIVcpzPts.

DISCUSSION

During the early phase of HIV-1 infection, capsid inhibitors such as PF74 either stabilize or disintegrate the core, depending on the concentrations applied (31, 32, 77, 78). The mechanism of inhibition by capsid inhibitors is currently poorly defined. Cyclophilin A was found to enhance the antiviral activity of PF74, but also to protect HIV-1 against high concentrations of PF74 (32, 33). The CYPA binding loop in capsid does not overlap with the PF74 binding site (Fig. 2A, 3) and, thus, a model of how CYPA regulates PF74 activity is not straightforward. However, the binding site of PF74 in the assembled capsid hexamers and pentamers overlaps with the binding sites of the cellular co-factors CPSF6 and NUP153, implicating a competition of PF74 and these cellular co-factors for the same binding groove (19, 29, 30, 33, 35, 78-80).

While the CYPA interaction with HIV-1 affects many different aspects of HIV-1 biology (18, 32, 51-60), recent studies concluded that the pathway most affected by CYPA inhibitions in cell lines is viral nuclear entry (61, 81). By comparing the permissivity of human cells to SIVs of chimpanzee, we found that HeLa cells are much less permissive to these viruses than HOS cells. Treating HeLa cells with CsA or using CYPA KD HeLa cells reverted the reduced permissiveness to SIVcpz. Our data on the CYPA capsid interaction collectively suggest that HIV-1 and SIVcpz GAG proteins interact with CYPA similarly despite differences in their CYPA-binding loop. In addition to CYPA, we tested the two SIVcpz viruses sensitivity to the anti-HIV-1 factors CPSF6-358, PF74, and PF57, as well as the potent capsid inhibitor GS-CA1. Expression of the truncated CPSF6 in the form of CPSF6-358 in human HOS cells repressed HIV-1 infections, which is consistent with previous observations (17, 33, 54, 82-84). Similarly,

but more moderately, CPSF6-358 reduced the infectivity of SIVcpzPtt. However, SIVcpzPts escaped the restriction by CPSF6-358 in HOS WT and in CYPA KO cells. Employing binding mode models of CPSF6 bound to all three CA proteins revealed that CPSF6 binding to HIV-1 CA and SIVcpzPtt CA is similar, whereas differential binding may be expected in the case of SIVcpzPts CA. These results parallel experimental ones in that HIV-1 and SIVcpzPtt, but not SIVcpzPts, was inhibited by CPSF6-358 expression.

The investigation of PF74 and related capsid inhibitors (PF57, GS-CA1) confirmed that SIVcpz and HIV-1 have intrinsic biological differences that have not been observed previously. These three viruses respond differently to capsid inhibitors in a cell-type dependent manner. HIV-1 was sensitive to PF57, PF74, and GS-CA1 and was inhibited 250- to 500-fold in HOS, HeLa cells, FRhL-2 and CRFK cells. SIVcpz viruses showed a similar sensitivity only in HOS and CRFK cells; in addition, SIVcpzPtt was sensitive to capsid inhibitors in HeLa cells. However, both SIVcpz viruses showed resistance in FRhL-2 cells and were inhibited only 2-fold at maximum drug concentration; in addition, SIVcpzPts was resistant in HeLa cells. Importantly, the capsid inhibitors were also inactive against SIVcpzPts in human macrophages and PBMCs, and SIVcpzPtt in PBMCs, while SIVcpzPtt was partially (2-fold) sensitive in macrophages.

Because SIVcpz viruses are not generally resistant to this type of inhibitors, we concluded that the antiviral activity of the capsid inhibitors depends on cellular infection pathways or the specific binding of a cellular protein. In particular, the finding that PF74 cannot interfere with SIVcpz infection in human PBMCs suggests that the results obtained with the cell lines are of biological relevance. Structural modelling of the PF74 interaction with CA proteins

revealed that the binding sites are identical in HIV-1 CA vs. SIVcpzPtt CA and highly similar for HIV-1 CA vs. SIVcpzPts, suggesting that that binding is highly similar to the three proteins. This suggestion was corroborated by effective binding energy computations, which are indistinguishable within chemical accuracy. These results are consistent with similar sensitivity of all three viruses to PF74 in human HOS cells.

The PF74 inhibition curve of HIV-1 in HeLa cells was described as being triphasic with two inhibitory phases flanking a plateau phase (19, 29, 33, 60). Here, we identified that the PF74 inhibition curve of HIV-1 in HeLa cells is only one of several different inhibition curves that capsid inhibitors can generate. Moreover, by testing capsid inhibitors against HIV-1, SIVcpzPtt and SIVcpzPts in CsA-treated cells or in cells with CYPA KO or deficiency, we obtained a complex interaction pattern that suggests that, in some cell types and specifically for SIVcpzPts, CYPA is an important antagonist of PF74-type capsid inhibitors. Our results in HeLa cells demonstrate that the functional inactivation of CYPA by CsA at low PF74 concentrations differentially affects the antiviral activity of the capsid inhibitors. However, at high PF74 levels, CsA treatment reverted the resistance of SIVcpzPts to PF74 and further enhanced the sensitivity of HIV-1 and SIVcpzPtt. We also tested how SIVcpz and HIV-1 reacted to capsid inhibitors in HOS.CYPA KO and HeLa.CYPA KD cells. The virus inhibition curves of PF57 or PF74 in HOS or HeLa cells lacking CYPA showed either no change, 2-4-fold lower antiviral activity, or slightly enhanced inhibition. The most striking observation was the total loss of resistance to capsid inhibitors of SIVcpzPts in HeLa cells due to CYPA KD. SIVcpzPts also lost its resistance to PF74 in HeLa cells when the virus was mutated in the CYPA-binding loop. This G89V mutation did not affect the sensitivity of HIV-1 to PF74 but further increased PF74's antiviral activity against SIVcpzPtt. These data suggest a diverse and

elaborate pattern of regulation of the antiviral capsid inhibitor activity by CYPA. However, in HeLa cells, CYPA has a clear protective role for SIVcpzPts against PF74 and PF57 at all drug concentrations.

The activity of PF74 and related compounds likely depends on the nuclear import of HIV-1 via NUP153, NUP358, and CPSF6 (1, 17-19, 33). HIV-1 variants that are more resistant to PF74's antiviral activity, but still bind the drug, are less dependent on NUP153 utilization (32, 33, 80). Knockdown of NUP153 in HeLa and HOS cells caused a 10-fold reduced capacity of PF74 to inhibit HIV-1 with residual antiviral activity at high drug concentrations (19, 33). The knockdown of CPSF6 did not affect high concentrations of PF74 but reduced the antiviral activity of the capsid inhibitor when applied at lower concentrations (33). These data, together with our findings, lead us to postulate that SIVcpz viruses – in particular SIVcpzPts - infects at least some cell types via a pathway that is independent of NUP153, NUP358, and CPSF6, consistent with recent findings describing a heterogeneity of nuclear pore complexes influencing HIV-1 infection (6, 85). We further speculate that during SIVcpz adaptation to humans, the capacity to use alternative nuclear entry pathways was lost for unknown reasons. Whether the nuclear entry pathway of SIVcpz viruses that can escape PF74 inhibition involves CYPA or CPSF6 requires further study.

MATERIAL AND METHODS

Plasmids. The murine leukemia virus (MLV) packaging construct pHIT60, which encodes the *gag-pol* of Moloney MLV was provided by Jonathan Stoye (86). SIVcpzPts clone TAN1.910 ((87), GenBank AF447763) was obtained from the NIH AIDS Reagent Program (Germantown, USA). SIVcpzPtt clone MB897 ((88), GenBank JN835461) was kindly provided by Frank Kirchhoff. HIV-1 vector pSIN.PPT.CMV.Luc.IRES.GFP expresses firefly luciferase and GFP (89). The HIV-1 construct psPAX2 was obtained from the NIH AIDS Reagent Program (Cat# 11348), pRSV-Rev, pMDLg/pRRE and pMD.G (VSV-G) have been described (90). HIV-1 capsid mutants were produced as follows: Using fusion PCR, the region flanking Eco72I (PmlI) and MunI (MfeI) in pMDLg/pRRE was amplified at the same time introducing G89V (56), N74D (54) or A77V (72) mutations in the capsid and cloned into pMDLg/pRRE plasmid digested by Eco72I (PmlI) and MunI (MfeI) (Thermo Fischer Scientific, Langenselbold, Germany). Using fusion PCR, SIVcpzPtt region flanking SacII and AleI (Thermo Fischer Scientific), SIVcpzPts region between NruI and BoxI (Thermo Fischer Scientific) restriction sites were amplified with introduction of G89V mutation in the capsids. Sequencing confirmed the desired mutations. This approach generated the pMDLg/pRRE.G89V, pMDLg/pRRE.N74D, and pMDLg/pRRE.A77V HIV-1 but also SIVcpzPtt.nanoluciferase.G89V and SIVcpzPts.nanoluciferase.G89V CA mutants. To generate GST-tagged human CYPA, CYPA cDNA with HindIII and BamHI sites was cloned in GST-containing pkMyc vector digested with the same enzymes (Thermo Fisher Scientific) to generate pkMyc.CYPA.GST. SIVcpzPtt MB897-nanoluciferase and SIVcpzPts TAN1-nanoluciferase have been described (42). To generate pLNCX2.CPSF6-358, NotI and XhoI digested HA-tagged CPSF6-358 cDNA (from plasmid LPCK-CPSF6-358.HA (17), a gift of Thomas Gramberg) was cloned in pLNCX2 (Takara

Bio Europe, Saint-Germain-en-Laye, France) digested with same restriction enzymes and positive clones were confirmed through sequencing.

Cells. Wild type HOS (ATCC CRL-1543, LGC Standards GmbH, Wesel, Germany), HeLa (ATCC CCL-2), HEK293T (ATCC CRL3216), OMK (637-69, ECACC, Sigma-Aldrich Chemie GmbH, Taufkirchen, Germany), CV-1 (ATCC CCL-70), CRFK (ATCC CCL-94), FRhL-2 (ATCCR CL-160) cells were maintained in Dulbecco's Modified Eagle's Medium (PAN-Biotech, Aidenbach, Germany) supplemented with 10% FBS, 2 mM L-glutamine and 100 U/ml penicillin/streptomycin at 37°C in a humidified atmosphere of 5% CO_2. For HOS and HeLa CYPA knockout cells, 2 µg/ml puromycin was added to the culture medium for selection. HOS cells expressing CPSF6-358 were selected under 300 µg/ml geneticin (Biochrom GmbH, Berlin, Germany). Human PBMCs and macrophages were isolated from whole blood, obtained from the university hospital of the Heinrich-Heine University Düsseldorf (ethical approval study number 3180). PBMCs were cultured in RPMI supplemented with 10 µg phytohemagglutinin (PHA) and later with 30 U/ml interleukin-2 and macrophages were maintained in RPMI containing 1000 U/ml Monocyte-Colony Stimulating Factor (M-CSF).

HIV-1 and SIVcpz reporter viral particle production. HIV-1 VSV-G pseudotyped viral particles were produced in a six well-plate by transfection of HEK293T cells with 200 ng of pMD.G, 800 ng of pSIN.PPT.CMV.Luc.IRES.GFP, 350 ng of pRSV-Rev and 800 ng of pMDLg/pRRE wild type or pMDLg/pRRE.N74D or pMDLg/pRRE.A77V. To produce SIVcpzPtt-nanoluciferase or SIVcpzPts-nanoluciferase viruses, 2250 ng of either reporter plasmid plus 200 ng pMD.G were used to transfect HEK293T cells. 48 hours following transfection, supernatants were collected, centrifuged 5 min at 5000 rpm at 4^{o}C to pellet possible cells. Where needed, the

reverse transcriptase (RT) activity of viruses was quantified using the Cavidi HS lenti RT kit (Cavidi Tech, Uppsala, Sweden).

Generation of CYPA knockout cells. pLentiCRISPRv2 plasmid construct for CYPA knockout was constructed according to previously described protocols (91-93). Complementary oligonucleotides (5'CACCGTTCTTCGACATTGCCGTCGA3', 5'AAACTCGACGGCAATGTCGAAGAA3' for HeLa cells and 5'CACCGGACAAGGTCCCAAAGACAGC3', 5'AAACGCTGTCTTTGGGACCTTGTCC3' for HOS cells) containing the specific human CYPA sgRNA sequences were ligated in a BsmBI digested pLentiCRISPRv2 to generate the functional transfer vector. LentiCRISPRv2 plasmid lacking sgRNA sequence was used as empty vector control. Transfection of HEK293T cells with pLentiCRISPRv2 transfer vector containing CYPA knockout sgRNA, packaging plasmid psPAX2, and VSV-G plasmid generated VSV-G pseudotyped viral particles, which were used to transduce HeLa or HOS cells for three days. Transduced cells were then selected under 2 µg/ml puromycin. While this process almost completely removed CYPA in HeLa cells, the protein only reduced it in HOS cells. Using flow cytometry (FACS ARIA III Sorter, BD, Heidelberg, Germany), single cells were isolated of HOS cells with anti CYPA constructs in wells of a 96-well plate for single clones. Gene knockout or knockdown in cell pools and clones was confirmed by immunoblot.

Generation of CPSF6-358 expressing cells. 1150 ng of the pLNCX2.CPSF6-358 construct together with 1150 ng of pHIT60 and 200 ng pMD.G were used to produce gammaretroviral particles in HEK293T cells and these particles were used to transduce wild type or CYPA knockout HOS cells for expression of CPSF6-358-HA. HOS cells expressing CPSF6-358 were

selected using 300 µg/ml geneticin (Biochrom GmbH). CPSF6-358 protein expression was analyzed by immunoblot. Cells expressing empty pLNCX2 or LentiCRISPRv2 vector were used as controls.

Single round infection. 10 x 10^3 cells were seeded into 96-well plates and infection was performed the following day. PF-3450074 (PF74 (8), (AOBIOUS, Biotrend, Cologne, Germany), GS-CA1 (a gift of Gilead Sciences Foster City, USA), cyclosporin A (CsA, Sigma Aldrich) or PF-3759857 (PF57 (8)) were added to cells, two hours before infection and control infections were performed with DMSO. PF57 was obtained in two steps starting from N-Boc-L-phenylalanine. After 48 to 72 hours, firefly luciferase activity was measured with the Steady-Glo Luciferase system (Promega, Mannheim, Germany) according to the manufacturer's instructions, on a MicroLumat Plus luminometer (Berthold Detection Systems, Pforzheim, Germany). For SIVcpz-nanoluciferase, cells were washed with phosphate-buffered saline (PBS) three times 48 hours after infection before lysis and luciferase measurement, in addition to medium change 24 hours following infection, to eliminate the effect of extracellular nanoluciferase in the supernatant. Nanoluciferase activity was measured with Nano-Glo Luciferase system (Promega) on a MicroLumat Plus luminometer (Berthold Detection Systems). Each experiment was performed in triplicates and at least three times.

Cyclophilin A encapsidation. HEK293T cells were seeded in 6-well plates (10^6 cells per well) one day before transfection. Two hours before transfection, 2.5 µM CsA or DMSO for controls were added to cells. Transfection was done as follows: Lipofectamine 2000 (Thermo Fisher Scientific, according to manufacturer's instructions) was used to complex a total of

2500 ng of plasmid DNA for delivery into cells. For SIVcpz, 2300 ng of the viral reporter plasmid and 200 ng pMD.G VSV-G were used. In case of HIV-1, 200 ng of pMD.G, 975 ng of pSIN.PPT.CMV.Luc.IRES.GFP, 350 ng of pRSV-Rev and 975 ng of pMDLg/pRRE were used for transfection. 48 hours post-transfection, the supernatant was collected and viral concentration was done through 20% sucrose for 4 hours at 4 degrees and viral pellets were lysed using western blot lysis buffer.

Pulldown experiments. HEK293T cells were seeded in 6-well plates (10^6 cells per well) one day before transfection. Transfection was done as follows: Lipofectamine 2000 (Thermo Fisher Scientific) was used to complex a total of 2600 ng of plasmid DNA for delivery into cells. For SIVcpz, 1700 ng of the viral reporter plasmid, 200 ng pMD.G VSV-G, and 700 ng of pcMyc.CYPA.GST constituted a plasmid complex for transfection. For HIV-1, 200 ng of pMD.G, 700 ng of pSIN.PPT.CMV.Luc.IRES.GFP, 300 ng of pRSV-Rev and 700 ng of pMDLg/pRRE and 700 ng of pcMyc.CYPA.GST or 700 ng pk.GST for control were used. 700 ng of pk.GST or CYPA.GST together with 1900 ng of pcDNA3.1 were used for control. Six hours post-transfection, 5 or 10 µM CsA or control DMSO were added to cells. 48 h post-transfection, cells were lysed for 20 minutes on ice, followed by a 20 min centrifugation at maximum speed of a benchtop centrifuge at 4^oC. The supernatant of the cell lysate was added to GST-beads together with viral lysates (obtained after 4 h centrifugation under 20% sucrose at 4^oC) and incubated according to beads manufacturer's instructions (GE HealthCare Solingen, Germany). Protein complexes were eluted from the beads and subjected to immunoblot.

Immunoblot. Cells were lysed for 20 minutes on ice, using radio-immunoprecipitation assay (RIPA) buffer (25 mM Tris-HCl [pH 8.0], 137 mM NaCl, 1% NP-40, 1% glycerol, 0.5% sodium deoxycholate, 0.1% sodium dodecyl sulfate (SDS), 2 mM EDTA, and protease inhibitor cocktail set III [Calbiochem, Darmstadt, Germany]). The cell lysate was centrifuged at 14,800 rpm for 20 minutes at 4°C. Lysate protein denaturation was done for 5 minutes at 95°C in RotiLoad loading buffer (Roth, Karlsruhe, Germany), followed by western blot. CPSF6-358.HA was detected with mouse anti-HA (MMS-101P, Covance, Münster, Germany, 1:7500 dilution). Tubulin was detected using the anti-tubulin antibody (DM1A, mouse, monoclonal, Sigma-Aldrich, 1:20,000 dilution). CPSF6 was detected using an anti-CPSF6-antibody (Proteintech, Manchester, UK; rabbit, polyclonal, 1:500 dilution). For TRIM5α detection, an anti–TRIM5-antibody was used (cat# 143265, Cell Signalling TECHNOLOGY Europe B.V, Frankfurt, Germany; rabbit, monoclonal, 1:500 dilution). For NUP153 detection, an anti–NUP153-antibody was used (mouse monoclonal, 1:500 dilution, Santa Cruz Biotechnology, Heidelberg, Germany). An anti–NUP358 antibody (mouse monoclonal, 1:500 dilution, Abcam, Cambridge, UK) was used for NUP358 detection. For CYPA detection, an anti–CYPA antibody was used (Santa Cruz Biotechnology, mouse, monoclonal, 1:500 dilution). CYPA.GST was detected using mouse anti-GST (kindly donated by Reza Ahmadian), p24/p27 MAb AG3.0 (1:250 dilution) was used to detect capsid p24. Anti-mouse conjugated to horseradish peroxidase (1:10,000 dilution, NA931V, GE Healthcare) and anti-rabbit conjugated to horseradish peroxidase (1:10,000 dilution, NA9340V, GE Healthcare) were used as secondary antibodies. Signals were visualized using ECL prime reagent (GE Healthcare).

Modelling of HIV-1, SIVcpzPts, and SIVcpzPtt CA protein-ligand structures. For each CA protein, three monomeric structures were built with TopModel (94) and validated with TopScore (73), one for each ligand. In addition, CYPA was modelled with TopModel (see table 1 for used templates). Hexameric structures were then constructed by alignment to the crystal structure of the HIV-1 CA protein (PDB ID 4WYM (31)) using PyMOL 1.8. Finally, to generate three complex structures for each protein, ligands were inserted into the respective hexameric structures, using the position of PF74 from PDB ID 4XFZ (95), the position of CPSF6 from PDB ID 4WYM (31), and the position of CYPA from PDB ID 1FGL (96) after superimposing the protein parts. For PF74, which was subsequently investigated in the complex with the CA protein by molecular dynamics simulations and effective binding energy computations, the superimposing was performed six times, to place PF74 in every binding pocket of the hexamer. For investigating CPSF6 and CYPA, for which only static complex structures were analyzed, this procedure was performed for one binding site only. Residues within 6 Å around the ligands were considered part of the binding pocket. **Molecular dynamics simulations of PF74 bound to HIV-1, SIVcpzPts, and SIVcpzPtt CA proteins.** System setup: For five replica per hexameric CA protein-PF74 structure, molecular dynamics (MD) simulations were performed with the Amber18 software package, resulting in total, 3 x 5 MD simulations. Protonation states of protein residues and ligands were adjusted according to pH 7.4 using HTMD 1.12 (97). Atomic point charges of PF74 were generated following the RESP procedure (98, 99), using antechamber (100) and GAUSSIAN16 (Rev. A.03) (101) at the HF/6-31G* level of theory. For the protein part, ff14SB force field parameters were used (102), for the ligand gaff2 force field parameters. Using tLEaP, the systems were solvated by an octahedral box of TIP3P water (103) such that the minimal distance between the box edge and any solute atom is 17 Å, and potassium ions were added

615 to neutralize the charge of the systems (103). Thermalization and production: Initially, the
616 simulation systems (including solute and solvent) were energy-minimized using 10,000 steps
617 of steepest descent minimization, followed by 10,000 steps of conjugate gradient
618 minimization, applying positional restraints on protein and ligand atoms with a force
619 constant of 20 kcal mol^{-1} $Å^{-2}$. Second, the same minimization scheme was applied, now using
620 positional restraints with a force constant of 20 kcal mol^{-1} $Å^{-2}$ on the protein atoms only.
621 Finally, the systems were minimized using 20,000 steps of steepest descent minimization,
622 followed by 20,000 steps of conjugate gradient minimization, applying no restraints. Using
623 NVT MD simulations, the systems were heated to 300 K using a constant heating rate over
624 210 ps and simulated for further 70 ps at this temperature with positional restraints with a
625 force constant of 10.0 kcal mol^{-1} $Å^{-2}$ on protein and PF74 atoms. Subsequently, the density of
626 the systems was adjusted using NPT MD simulations and applying the Berendsen barostat
627 for 1,300 ps, with positional restraints with a force constant of 2.0 kcal mol^{-1} $Å^{-2}$ on protein
628 and PF74 atoms, followed by a final equilibration step of 1720 ps in the NVT ensemble. For
629 production, NVT MD simulations were performed for 200 ns, yielding an aggregate
630 simulation time of 3 x 5 x 200 ns = 3 μs, and coordinates were stored every 100 ps. For all
631 simulations, the Langevin thermostat with a collision frequency of 2 ps^{-1} was used.
632 Minimization and heating were performed on CPUs, equilibration, and production on GPUs
633 with PMEMD (104). Calculation of effective binding energies: Effective binding energies were
634 calculated using MMPBSA.py (74) from AmberTools19. For the calculation, the hexamers
635 were split into six dimers containing one PF74 molecule each in the corresponding binding
636 interface. Hence, 30 dimers per isoform were analyzed, corresponding to a total of 60,000
637 frames per isoform. We applied the 1-trajectory MM-PBSA approach, in which the snapshots
638 of the complex, protein, and ligand are extracted from a single MD simulation of the

639 complex (75). The polar part of the solvation free energy was computed with the linearized
640 Poisson-Boltzmann equation using an internal dielectric constant of 4 and an external one of
641 80. The nonpolar part was computed using as a surface tension of 0.0378 kcal mol-1 Å-2
642 (105). To avoid any additional uncertainty in our calculations, we neglected contributions
643 due to changes in the configurational entropy upon complex formation (106, 107).

644 The effective binding energies ($\Delta G_{\text{effective}}$) were averaged over five replica each containing six
645 binding pockets ($\overline{\Delta G}_{\text{effective}}$). The distribution of $\Delta G_{\text{effective}}$ values is Gaussian, and no particular
646 trends were observed over the simulation times. The SEM (Standard Error of the Mean) over
647 the 30 independent calculations for a system (SEM_{all}) was calculated by error propagation
648 according to eq. (1):

$$SEM_{\text{all}} = \frac{1}{5\text{x}6}\sqrt{\sum_{i=1}^{5}\sum_{j=1}^{6} SEM_{i,j}{}^{2}} \qquad (1)$$

649 In all cases, the statistical uncertainty (SEM_{all}) is < 0.015 kcal mol^{-1} and, hence, below the
650 chemical accuracy of 1 kcal mol^{-1}, which is the expected accuracy in an optimal case (76).

651

652 **Protein sequence alignment.** The alignment was generated with MAFFT (108) in JalView
653 (109). JalView was also used to generate the Weblogos. The following randomly picked
654 sequences (GenBank accession numbers) were included in the analyzes: HIV-1 M diverse
655 subtypes (A04321, AB023804, AB032740, AB049811, AB097865, AB098330, AB221005,
656 AB221005, AB253421, AB485636, AB485638, AB485643, AB485646, AB485648, AB485656,
657 AB485660, AB485662, AB703607, AB731663, AF110963, AF190127, in addition the sequence
658 of the plasmid pMDLg/pRRE), SIVcpzPtt (AF382828, AF103818.1, AF115393, AJ271369,
659 AY169968, DQ373063, DQ373064, DQ373065, DQ373066, EF535993, FR686510, FR686511,

GQ217539, JN091690, JN835461, JN835462, JX178450, X52154), and SIVcpzPts (AF447763, DQ374657, DQ374658, EF394356, EF394357, EF394358, JN091691, JN835460, JQ768416, JQ866001, SIU42720).

Statistics. Statistical tests for significance (p-value <0.05) were performed with GraphPad Prism 5.

ACKNOWLEDGEMENTS

We thank Wioletta Hörschken and Björn Wefers for excellent technical assistance. We thank Reza Ahmadian, Gilead Sciences, Thomas Gramberg, Beatrice H. Hahn, Frank Kirchhoff, Daniel Sauter, Heiner Schaal, Jonathan P. Stoye, Greg Towers, and Stephen R. Yant for reagents and Felipe Diaz-Griffero and Neeltje Kootstra for discussion. The following reagents were obtained through the NIH AIDS Research and Reference Reagent Program, Division of AIDS, NIAID, NIH: psPAX2 (Cat# 11348) from Didier Trono, SIVcpz TAN1.910 infectious molecular clone (Cat #11496) from Jun Takehisa, Matthias H. Kraus and Beatrice H. Hahn. APT is supported by German Academic Exchange Service (DAAD). ZZ was supported by China Scholarship Council (CSC). CM is supported by the Heinz-Ansmann foundation for AIDS research. HG is grateful for computational support and infrastructure provided by the "Zentrum für Informations- und Medientechnologie" (ZIM) at the Heinrich-Heine-University Düsseldorf and the computing time provided by the John von Neumann Institute for Computing (NIC) to HG on the supercomputer JUWELS at Jülich Supercomputing Centre (JSC) (user ID: HKF7).

REFERENCES

1. **Bejarano DA, Peng K, Laketa V, Borner K, Jost KL, Lucic B, Glass B, Lusic M, Muller B, Krausslich HG.** 2019. HIV-1 nuclear import in macrophages is regulated by CPSF6-capsid interactions at the nuclear pore complex. Elife **8**.
2. **Arhel NJ, Souquere-Besse S, Munier S, Souque P, Guadagnini S, Rutherford S, Prevost MC, Allen TD, Charneau P.** 2007. HIV-1 DNA Flap formation promotes uncoating of the pre-integration complex at the nuclear pore. EMBO J **26:**3025-3037.
3. **Francis AC, Melikyan GB.** 2018. Single HIV-1 Imaging Reveals Progression of Infection through CA-Dependent Steps of Docking at the Nuclear Pore, Uncoating, and Nuclear Transport. Cell Host Microbe **23:**536-548 e536.
4. **Mamede JI, Cianci GC, Anderson MR, Hope TJ.** 2017. Early cytoplasmic uncoating is associated with infectivity of HIV-1. Proc Natl Acad Sci U S A **114:**E7169-E7178.
5. **Burdick RC, Li C, Munshi M, Rawson JMO, Nagashima K, Hu WS, Pathak VK.** 2020. HIV-1 uncoats in the nucleus near sites of integration. Proc Natl Acad Sci U S A **117:**5486-5493.
6. **Dharan A, Bachmann N, Talley S, Zwikelmaier V, Campbell EM.** 2020. Nuclear pore blockade reveals that HIV-1 completes reverse transcription and uncoating in the nucleus. Nat Microbiol doi:10.1038/s41564-020-0735-8.
7. **Zurnic Bönisch I, Dirix L, Lemmens V, Borrenberghs D, De Wit F, Vernaillen F, Rocha S, Christ F, Hendrix J, Hofkens J, Debyser Z.** 2020. Capsid-Labelled HIV To Investigate the Role of Capsid during Nuclear Import and Integration. J Virol **94**.
8. **Blair WS, Pickford C, Irving SL, Brown DG, Anderson M, Bazin R, Cao J, Ciaramella G, Isaacson J, Jackson L, Hunt R, Kjerrstrom A, Nieman JA, Patick AK, Perros M, Scott AD, Whitby K, Wu H, Butler SL.** 2010. HIV capsid is a tractable target for small molecule therapeutic intervention. PLoS Pathog **6:**e1001220.
9. **Lamorte L, Titolo S, Lemke CT, Goudreau N, Mercier JF, Wardrop E, Shah VB, von Schwedler UK, Langelier C, Banik SS, Aiken C, Sundquist WI, Mason SW.** 2013. Discovery of novel small-molecule HIV-1 replication inhibitors that stabilize capsid complexes. Antimicrob Agents Chemother **57:**4622-4631.
10. **Franke EK, Yuan HE, Luban J.** 1994. Specific incorporation of cyclophilin A into HIV-1 virions. Nature **372:**359-362.
11. **Thali M, Bukovsky A, Kondo E, Rosenwirth B, Walsh CT, Sodroski J, Gottlinger HG.** 1994. Functional association of cyclophilin A with HIV-1 virions. Nature **372:**363-365.
12. **Stremlau M, Owens CM, Perron MJ, Kiessling M, Autissier P, Sodroski J.** 2004. The cytoplasmic body component TRIM5alpha restricts HIV-1 infection in Old World monkeys. Nature **427:**848-853.
13. **Kane M, Yadav SS, Bitzegeio J, Kutluay SB, Zang T, Wilson SJ, Schoggins JW, Rice CM, Yamashita M, Hatziioannou T, Bieniasz PD.** 2013. MX2 is an interferon-induced inhibitor of HIV-1 infection. Nature **502:**563-566.
14. **Goujon C, Moncorge O, Bauby H, Doyle T, Ward CC, Schaller T, Hue S, Barclay WS, Schulz R, Malim MH.** 2013. Human MX2 is an interferon-induced post-entry inhibitor of HIV-1 infection. Nature **502:**559-562.
15. **Brass AL, Dykxhoorn DM, Benita Y, Yan N, Engelman A, Xavier RJ, Lieberman J, Elledge SJ.** 2008. Identification of host proteins required for HIV infection through a functional genomic screen. Science **319:**921-926.
16. **König R, Zhou Y, Elleder D, Diamond TL, Bonamy GM, Irelan JT, Chiang CY, Tu BP, De Jesus PD, Lilley CE, Seidel S, Opaluch AM, Caldwell JS, Weitzman MD, Kuhen KL, Bandyopadhyay S, Ideker T, Orth AP, Miraglia LJ, Bushman FD, Young JA, Chanda SK.** 2008. Global analysis of host-pathogen interactions that regulate early-stage HIV-1 replication. Cell **135:**49-60.
17. **Lee K, Ambrose Z, Martin TD, Oztop I, Mulky A, Julias JG, Vandegraaff N, Baumann JG, Wang R, Yuen W, Takemura T, Shelton K, Taniuchi I, Li Y, Sodroski J, Littman DR, Coffin JM, Hughes SH, Unutmaz D, Engelman A, KewalRamani VN.** 2010. Flexible use of nuclear import pathways by HIV-1. Cell Host Microbe **7:**221-233.

18. **Schaller T, Ocwieja KE, Rasaiyaah J, Price AJ, Brady TL, Roth SL, Hue S, Fletcher AJ, Lee K, KewalRamani VN, Noursadeghi M, Jenner RG, James LC, Bushman FD, Towers GJ.** 2011. HIV-1 capsid-cyclophilin interactions determine nuclear import pathway, integration targeting and replication efficiency. PLoS Pathog **7:**e1002439.
19. **Matreyek KA, Yucel SS, Li X, Engelman A.** 2013. Nucleoporin NUP153 phenylalanine-glycine motifs engage a common binding pocket within the HIV-1 capsid protein to mediate lentiviral infectivity. PLoS Pathog **9:**e1003693.
20. **Mamede JI, Sitbon M, Battini JL, Courgnaud V.** 2013. Heterogeneous susceptibility of circulating SIV isolate capsids to HIV-interacting factors. Retrovirology **10:**77.
21. **Jimenez-Guardeno JM, Apolonia L, Betancor G, Malim MH.** 2019. Immunoproteasome activation enables human TRIM5alpha restriction of HIV-1. Nat Microbiol **4:**933-940.
22. **Ohainle M, Kim K, Komurlu Keceli S, Felton A, Campbell E, Luban J, Emerman M.** 2020. TRIM34 restricts HIV-1 and SIV capsids in a TRIM5alpha-dependent manner. PLoS Pathog **16:**e1008507.
23. **Selyutina A, Persaud M, Simons LM, Bulnes-Ramos A, Buffone C, Martinez-Lopez A, Scoca V, Di Nunzio F, Hiatt J, Marson A, Krogan NJ, Hultquist JF, Diaz-Griffero F.** 2020. Cyclophilin A Prevents HIV-1 Restriction in Lymphocytes by Blocking Human TRIM5alpha Binding to the Viral Core. Cell Rep **30:**3766-3777 e3766.
24. **De Iaco A, Luban J.** 2011. Inhibition of HIV-1 infection by TNPO3 depletion is determined by capsid and detectable after viral cDNA enters the nucleus. Retrovirology **8:**98.
25. **Ning J, Zhong Z, Fischer DK, Harris G, Watkins SC, Ambrose Z, Zhang P.** 2018. Truncated CPSF6 Forms Higher-Order Complexes That Bind and Disrupt HIV-1 Capsid. J Virol **92**.
26. **Merindol N, El-Far M, Sylla M, Masroori N, Dufour C, Li JX, Cherry P, Plourde MB, Tremblay C, Berthoux L.** 2018. HIV-1 capsids from B27/B57+ elite controllers escape Mx2 but are targeted by TRIM5alpha, leading to the induction of an antiviral state. PLoS Pathog **14:**e1007398.
27. **Maillard PV, Zoete V, Michielin O, Trono D.** 2011. Homology-based identification of capsid determinants that protect HIV1 from human TRIM5alpha restriction. J Biol Chem **286:**8128-8140.
28. **Busnadiego I, Kane M, Rihn SJ, Preugschas HF, Hughes J, Blanco-Melo D, Strouvelle VP, Zang TM, Willett BJ, Boutell C, Bieniasz PD, Wilson SJ.** 2014. Host and viral determinants of Mx2 antiretroviral activity. J Virol **88:**7738-7752.
29. **Price AJ, Jacques DA, McEwan WA, Fletcher AJ, Essig S, Chin JW, Halambage UD, Aiken C, James LC.** 2014. Host cofactors and pharmacologic ligands share an essential interface in HIV-1 capsid that is lost upon disassembly. PLoS Pathog **10:**e1004459.
30. **Price AJ, Fletcher AJ, Schaller T, Elliott T, Lee K, KewalRamani VN, Chin JW, Towers GJ, James LC.** 2012. CPSF6 defines a conserved capsid interface that modulates HIV-1 replication. PLoS Pathog **8:**e1002896.
31. **Bhattacharya A, Alam SL, Fricke T, Zadrozny K, Sedzicki J, Taylor AB, Demeler B, Pornillos O, Ganser-Pornillos BK, Diaz-Griffero F, Ivanov DN, Yeager M.** 2014. Structural basis of HIV-1 capsid recognition by PF74 and CPSF6. Proc Natl Acad Sci U S A **111:**18625-18630.
32. **Shi J, Zhou J, Shah VB, Aiken C, Whitby K.** 2011. Small-molecule inhibition of human immunodeficiency virus type 1 infection by virus capsid destabilization. J Virol **85:**542-549.
33. **Saito A, Ferhadian D, Sowd GA, Serrao E, Shi J, Halambage UD, Teng S, Soto J, Siddiqui MA, Engelman AN, Aiken C, Yamashita M.** 2016. Roles of Capsid-Interacting Host Factors in Multimodal Inhibition of HIV-1 by PF74. J Virol **90:**5808-5823.
34. **Hulme AE, Kelley Z, Foley D, Hope TJ.** 2015. Complementary Assays Reveal a Low Level of CA Associated with Viral Complexes in the Nuclei of HIV-1-Infected Cells. J Virol **89:**5350-5361.
35. **Balasubramaniam M, Zhou J, Addai A, Martinez P, Pandhare J, Aiken C, Dash C.** 2019. PF74 Inhibits HIV-1 Integration by Altering the Composition of the Preintegration Complex. J Virol **93**.

787 36. **Carnes SK, Sheehan JH, Aiken C.** 2018. Inhibitors of the HIV-1 capsid, a target of opportunity.
788 Curr Opin HIV AIDS **13:**359-365.
789 37. **Singh K, Gallazzi F, Hill KJ, Burke DH, Lange MJ, Quinn TP, Neogi U, Sonnerborg A.** 2019. GS-
790 CA Compounds: First-In-Class HIV-1 Capsid Inhibitors Covering Multiple Grounds. Front
791 Microbiol **10:**1227.
792 38. **Yant SR, Mulato A, Hansen D, Tse WC, Niedziela-Majka A, Zhang JR, Stepan GJ, Jin D, Wong**
793 **MH, Perreira JM, Singer E, Papalia GA, Hu EY, Zheng J, Lu B, Schroeder SD, Chou K,**
794 **Ahmadyar S, Liclican A, Yu H, Novikov N, Paoli E, Gonik D, Ram RR, Hung M, McDougall**
795 **WM, Brass AL, Sundquist WI, Cihlar T, Link JO.** 2019. A highly potent long-acting small-
796 molecule HIV-1 capsid inhibitor with efficacy in a humanized mouse model. Nat Med
797 **25:**1377-1384.
798 39. **Twizerimana AP, Scheck R, Häussinger D, Münk C.** 2018. Post-entry restriction factors of
799 SIVcpz. Future Virology **13:**727-745.
800 40. **Sharp PM, Hahn BH.** 2010. The evolution of HIV-1 and the origin of AIDS. Philos Trans R Soc
801 Lond B Biol Sci **365:**2487-2494.
802 41. **Gao F, Bailes E, Robertson DL, Chen Y, Rodenburg CM, Michael SF, Cummins LB, Arthur LO,**
803 **Peeters M, Shaw GM, Sharp PM, Hahn BH.** 1999. Origin of HIV-1 in the chimpanzee Pan
804 troglodytes troglodytes. Nature **397:**436-441.
805 42. **Zhang Z, Gu Q, de Manuel Montero M, Bravo IG, Marques-Bonet T, Häussinger D, Münk C.**
806 2017. Stably expressed APOBEC3H forms a barrier for cross-species transmission of simian
807 immunodeficiency virus of chimpanzee to humans. PLoS Pathog **13:**e1006746.
808 43. **Sauter D, Schindler M, Specht A, Landford WN, Munch J, Kim KA, Votteler J, Schubert U,**
809 **Bibollet-Ruche F, Keele BF, Takehisa J, Ogando Y, Ochsenbauer C, Kappes JC, Ayouba A,**
810 **Peeters M, Learn GH, Shaw G, Sharp PM, Bieniasz P, Hahn BH, Hatziioannou T, Kirchhoff F.**
811 2009. Tetherin-driven adaptation of Vpu and Nef function and the evolution of pandemic and
812 nonpandemic HIV-1 strains. Cell HostMicrobe **6:**409-421.
813 44. **Kratovac Z, Virgen CA, Bibollet-Ruche F, Hahn BH, Bieniasz PD, Hatziioannou T.** 2008.
814 Primate lentivirus capsid sensitivity to TRIM5 proteins. J Virol **82:**6772-6777.
815 45. **Meier K, Jaguva Vasudevan AA, Zhang Z, Bahr A, Kochs G, Häussinger D, Münk C.** 2018.
816 Equine MX2 is a restriction factor of equine infectious anemia virus (EIAV). Virology **523:**52-
817 63.
818 46. **McEwan WA, Schaller T, Ylinen LM, Hosie MJ, Towers GJ, Willett BJ.** 2009. Truncation of
819 TRIM5 in the Feliformia explains the absence of retroviral restriction in cells of the domestic
820 cat. JVirol **83:**8270-8275.
821 47. **Bieniasz PD.** 2004. Intrinsic immunity: a front-line defense against viral attack. Nat Immunol
822 **5:**1109-1115.
823 48. **Münk C, Brandt SM, Lucero G, Landau NR.** 2002. A dominant block to HIV-1 replication at
824 reverse transcription in simian cells. ProcNatlAcadSciUSA **99:**13843-13848.
825 49. **Cowan S, Hatziioannou T, Cunningham T, Muesing MA, Gottlinger HG, Bieniasz PD.** 2002.
826 Cellular inhibitors with Fv1-like activity restrict human and simian immunodeficiency virus
827 tropism. Proc Natl Acad Sci U S A **99:**11914-11919.
828 50. **Besnier C, Takeuchi Y, Towers G.** 2002. Restriction of lentivirus in monkeys. Proc Natl Acad
829 Sci U S A **99:**11920-11925.
830 51. **Lu M, Hou G, Zhang H, Suiter CL, Ahn J, Byeon IJ, Perilla JR, Langmead CJ, Hung I, Gor'kov**
831 **PL, Gan Z, Brey W, Aiken C, Zhang P, Schulten K, Gronenborn AM, Polenova T.** 2015.
832 Dynamic allostery governs cyclophilin A-HIV capsid interplay. Proc Natl Acad Sci U S A
833 **112:**14617-14622.
834 52. **Liu Z, Pan Q, Ding S, Qian J, Xu F, Zhou J, Cen S, Guo F, Liang C.** 2013. The interferon-
835 inducible MxB protein inhibits HIV-1 infection. Cell Host Microbe **14:**398-410.
836 53. **Rasaiyaah J, Tan CP, Fletcher AJ, Price AJ, Blondeau C, Hilditch L, Jacques DA, Selwood DL,**
837 **James LC, Noursadeghi M, Towers GJ.** 2013. HIV-1 evades innate immune recognition
838 through specific cofactor recruitment. Nature **503:**402-405.

54. **Ambrose Z, Lee K, Ndjomou J, Xu H, Oztop I, Matous J, Takemura T, Unutmaz D, Engelman A, Hughes SH, KewalRamani VN.** 2012. Human immunodeficiency virus type 1 capsid mutation N74D alters cyclophilin A dependence and impairs macrophage infection. J Virol **86:**4708-4714.
55. **Qi M, Yang R, Aiken C.** 2008. Cyclophilin A-dependent restriction of human immunodeficiency virus type 1 capsid mutants for infection of nondividing cells. J Virol **82:**12001-12008.
56. **Sokolskaja E, Sayah DM, Luban J.** 2004. Target cell cyclophilin A modulates human immunodeficiency virus type 1 infectivity. J Virol **78:**12800-12808.
57. **Burse M, Shi J, Aiken C.** 2017. Cyclophilin A potentiates TRIM5alpha inhibition of HIV-1 nuclear import without promoting TRIM5alpha binding to the viral capsid. PLoS One **12:**e0182298.
58. **Sokolskaja E, Luban J.** 2006. Cyclophilin, TRIM5, and innate immunity to HIV-1. Curr Opin Microbiol **9:**404-408.
59. **Kootstra NA, Münk C, Tonnu N, Landau NR, Verma IM.** 2003. Abrogation of postentry restriction of HIV-1-based lentiviral vector transduction in simian cells. ProcNatlAcadSciUSA **100:**1298-1303.
60. **Shah VB, Shi J, Hout DR, Oztop I, Krishnan L, Ahn J, Shotwell MS, Engelman A, Aiken C.** 2013. The host proteins transportin SR2/TNPO3 and cyclophilin A exert opposing effects on HIV-1 uncoating. J Virol **87:**422-432.
61. **De Iaco A, Luban J.** 2014. Cyclophilin A promotes HIV-1 reverse transcription but its effect on transduction correlates best with its effect on nuclear entry of viral cDNA. Retrovirology **11:**11.
62. **Luban J, Bossolt KL, Franke EK, Kalpana GV, Goff SP.** 1993. Human immunodeficiency virus type 1 Gag protein binds to cyclophilins A and B. Cell **73:**1067-1078.
63. **Gamble TR, Vajdos FF, Yoo S, Worthylake DK, Houseweart M, Sundquist WI, Hill CP.** 1996. Crystal structure of human cyclophilin A bound to the amino-terminal domain of HIV-1 capsid. Cell **87:**1285-1294.
64. **Franke EK, Luban J.** 1996. Inhibition of HIV-1 replication by cyclosporine A or related compounds correlates with the ability to disrupt the Gag-cyclophilin A interaction. Virology **222:**279-282.
65. **Yin L, Braaten D, Luban J.** 1998. Human immunodeficiency virus type 1 replication is modulated by host cyclophilin A expression levels. J Virol **72:**6430-6436.
66. **Braaten D, Franke EK, Luban J.** 1996. Cyclophilin A is required for an early step in the life cycle of human immunodeficiency virus type 1 before the initiation of reverse transcription. J Virol **70:**3551-3560.
67. **Braaten D, Franke EK, Luban J.** 1996. Cyclophilin A is required for the replication of group M human immunodeficiency virus type 1 (HIV-1) and simian immunodeficiency virus SIV(CPZ)GAB but not group O HIV-1 or other primate immunodeficiency viruses. J Virol **70:**4220-4227.
68. **Hatziioannou T, Perez-Caballero D, Cowan S, Bieniasz PD.** 2005. Cyclophilin interactions with incoming human immunodeficiency virus type 1 capsids with opposing effects on infectivity in human cells. J Virol **79:**176-183.
69. **Mlynar E, Bevec D, Billich A, Rosenwirth B, Steinkasserer A.** 1997. The non-immunosuppressive cyclosporin A analogue SDZ NIM 811 inhibits cyclophilin A incorporation into virions and virus replication in human immunodeficiency virus type 1-infected primary and growth-arrested T cells. J Gen Virol **78 (Pt 4):**825-835.
70. **Saini M, Potash MJ.** 2006. Novel activities of cyclophilin A and cyclosporin A during HIV-1 infection of primary lymphocytes and macrophages. J Immunol **177:**443-449.
71. **Towers GJ, Hatziioannou T, Cowan S, Goff SP, Luban J, Bieniasz PD.** 2003. Cyclophilin A modulates the sensitivity of HIV-1 to host restriction factors. Nat Med **9:**1138-1143.

72. **Saito A, Henning MS, Serrao E, Dubose BN, Teng S, Huang J, Li X, Saito N, Roy SP, Siddiqui MA, Ahn J, Tsuji M, Hatziioannou T, Engelman AN, Yamashita M.** 2016. Capsid-CPSF6 Interaction Is Dispensable for HIV-1 Replication in Primary Cells but Is Selected during Virus Passage In Vivo. J Virol **90:**6918-6935.
73. **Mulnaes D, Gohlke H.** 2018. TopScore: Using Deep Neural Networks and Large Diverse Data Sets for Accurate Protein Model Quality Assessment. J Chem Theory Comput **14:**6117-6126.
74. **Miller BR, McGee TD, Swails JM, Homeyer N, Gohlke H, Roitberg AE.** 2012. MMPBSA.py: An Efficient Program for End-State Free Energy Calculations. J Chem Theory Comput **8:**3314-3321.
75. **Homeyer N, Gohlke H.** 2012. Free Energy Calculations by the Molecular Mechanics Poisson-Boltzmann Surface Area Method. Molecular Informatics **31:**114-122.
76. **Michel J, Essex JW.** 2010. Prediction of protein–ligand binding affinity by free energy simulations: assumptions, pitfalls and expectations. J Comp Aided Mol Des **24:**639-658.
77. **Rankovic S, Ramalho R, Aiken C, Rousso I.** 2018. PF74 Reinforces the HIV-1 Capsid To Impair Reverse Transcription-Induced Uncoating. J Virol **92**.
78. **Fricke T, Buffone C, Opp S, Valle-Casuso J, Diaz-Griffero F.** 2014. BI-2 destabilizes HIV-1 cores during infection and Prevents Binding of CPSF6 to the HIV-1 Capsid. Retrovirology **11:**120.
79. **Buffone C, Martinez-Lopez A, Fricke T, Opp S, Severgnini M, Cifola I, Petiti L, Frabetti S, Skorupka K, Zadrozny KK, Ganser-Pornillos BK, Pornillos O, Di Nunzio F, Diaz-Griffero F.** 2018. Nup153 Unlocks the Nuclear Pore Complex for HIV-1 Nuclear Translocation in Nondividing Cells. J Virol **92**.
80. **Zhou J, Price AJ, Halambage UD, James LC, Aiken C.** 2015. HIV-1 Resistance to the Capsid-Targeting Inhibitor PF74 Results in Altered Dependence on Host Factors Required for Virus Nuclear Entry. J Virol **89:**9068-9079.
81. **Lahaye X, Satoh T, Gentili M, Cerboni S, Silvin A, Conrad C, Ahmed-Belkacem A, Rodriguez EC, Guichou JF, Bosquet N, Piel M, Le Grand R, King MC, Pawlotsky JM, Manel N.** 2016. Nuclear Envelope Protein SUN2 Promotes Cyclophilin-A-Dependent Steps of HIV Replication. Cell Rep **15:**879-892.
82. **De Iaco A, Santoni F, Vannier A, Guipponi M, Antonarakis S, Luban J.** 2013. TNPO3 protects HIV-1 replication from CPSF6-mediated capsid stabilization in the host cell cytoplasm. Retrovirology **10:**20.
83. **Hori T, Takeuchi H, Saito H, Sakuma R, Inagaki Y, Yamaoka S.** 2013. A carboxy-terminally truncated human CPSF6 lacking residues encoded by exon 6 inhibits HIV-1 cDNA synthesis and promotes capsid disassembly. J Virol **87:**7726-7736.
84. **Lee K, Mulky A, Yuen W, Martin TD, Meyerson NR, Choi L, Yu H, Sawyer SL, Kewalramani VN.** 2012. HIV-1 capsid-targeting domain of cleavage and polyadenylation specificity factor 6. J Virol **86:**3851-3860.
85. **Kane M, Rebensburg SV, Takata MA, Zang TM, Yamashita M, Kvaratskhelia M, Bieniasz PD.** 2018. Nuclear pore heterogeneity influences HIV-1 infection and the antiviral activity of MX2. Elife **7**.
86. **Bock M, Bishop KN, Towers G, Stoye JP.** 2000. Use of a transient assay for studying the genetic determinants of Fv1 restriction. J Virol **74:**7422-7430.
87. **Takehisa J, Kraus MH, Decker JM, Li Y, Keele BF, Bibollet-Ruche F, Zammit KP, Weng Z, Santiago ML, Kamenya S, Wilson ML, Pusey AE, Bailes E, Sharp PM, Shaw GM, Hahn BH.** 2007. Generation of infectious molecular clones of simian immunodeficiency virus from fecal consensus sequences of wild chimpanzees. J Virol **81:**7463-7475.
88. **Bibollet-Ruche F, Heigele A, Keele BF, Easlick JL, Decker JM, Takehisa J, Learn G, Sharp PM, Hahn BH, Kirchhoff F.** 2012. Efficient SIVcpz replication in human lymphoid tissue requires viral matrix protein adaptation. J Clin Invest **122:**1644-1652.
89. **Bähr A, Singer A, Hain A, Vasudevan AA, Schilling M, Reh J, Riess M, Panitz S, Serrano V, Schweizer M, Konig R, Chanda S, Häussinger D, Kochs G, Lindemann D, Münk C.** 2015. Interferon but not MxB inhibits foamy retroviruses. Virology **488:**51-60.

90. **Dull T, Zufferey R, Kelly M, Mandel RJ, Nguyen M, Trono D, Naldini L.** 1998. A third-generation lentivirus vector with a conditional packaging system. JVirol **72:**8463-8471.
91. **Osei Kuffour E, Schott K, Jaguva Vasudevan AA, Holler J, Schulz WA, Lang PA, Lang KS, Kim B, Häussinger D, König R, Münk C.** 2018. USP18 (UBP43) Abrogates p21-Mediated Inhibition of HIV-1. J Virol **92**.
92. **Shalem O, Sanjana NE, Hartenian E, Shi X, Scott DA, Mikkelsen TS, Heckl D, Ebert BL, Root DE, Doench JG, Zhang F.** 2014. Genome-scale CRISPR-Cas9 knockout screening in human cells. Science **343:**84-87.
93. **Sanjana NE, Shalem O, Zhang F.** 2014. Improved vectors and genome-wide libraries for CRISPR screening. Nat Methods **11:**783-784.
94. **Mulnaes D, Porta N, Clemens R, Apanasenko I, Reiners J, Gremer L, Neudecker P, Smits SHJ, Gohlke H.** 2020. TopModel: Template-Based Protein Structure Prediction at Low Sequence Identity Using Top-Down Consensus and Deep Neural Networks. J Chem Theory Comput doi:10.1021/acs.jctc.9b00825.
95. **Gres AT, Kirby KA, KewalRamani VN, Tanner JJ, Pornillos O, Sarafianos SG.** 2015. STRUCTURAL VIROLOGY. X-ray crystal structures of native HIV-1 capsid protein reveal conformational variability. Science **349:**99-103.
96. **Zhao Y, Chen Y, Schutkowski M, Fischer G, Ke H.** 1997. Cyclophilin A complexed with a fragment of HIV-1 gag protein: insights into HIV-1 infectious activity. Structure **5:**139-146.
97. **Doerr S, Harvey MJ, Noé F, De Fabritiis G.** 2016. HTMD: High-Throughput Molecular Dynamics for Molecular Discovery. J Chem Theory Comput **12:**1845-1852.
98. **Bayly CI, Cieplak P, Cornell W, Kollman PA.** 1993. A well-behaved electrostatic potential based method using charge restraints for deriving atomic charges: the RESP model. The Journal of Physical Chemistry **97:**10269-10280.
99. **Wang J, Cieplak P, Kollman PA.** 2000. How well does a restrained electrostatic potential (RESP) model perform in calculating conformational energies of organic and biological molecules? J Comput Chem **21:**1049-1074.
100. **Wang J, Wang W, Kollman PA, Case DA.** 2006. Automatic atom type and bond type perception in molecular mechanical calculations. Journal of Molecular Graphics and Modelling **25:**247-260.
101. **Frisch MJ, Trucks GW, Schlegel HB, Scuseria GE, Robb MA, Cheeseman JR, Scalmani G, Barone V, Petersson GA, Nakatsuji H, Li X, Caricato M, Marenich AV, Bloino J, Janesko BG, Gomperts R, Mennucci B, Hratchian HP, Ortiz JV, Izmaylov AF, Sonnenberg JL, Williams, Ding F, Lipparini F, Egidi F, Goings J, Peng B, Petrone A, Henderson T, Ranasinghe D, Zakrzewski VG, Gao J, Rega N, Zheng G, Liang W, Hada M, Ehara M, Toyota K, Fukuda R, Hasegawa J, Ishida M, Nakajima T, Honda Y, Kitao O, Nakai H, Vreven T, Throssell K, Montgomery Jr. JA, Peralta JE, Ogliaro F, et al.** 2016. Gaussian 16 Rev. C.01, Wallingford, CT.
102. **Maier JA, Martinez C, Kasavajhala K, Wickstrom L, Hauser KE, Simmerling C.** 2015. ff14SB: Improving the Accuracy of Protein Side Chain and Backbone Parameters from ff99SB. J Chem Theory Comput **11:**3696-3713.
103. **Jorgensen WL, Chandrasekhar J, Madura JD, Impey RW, Klein ML.** 1983. Comparison of simple potential functions for simulating liquid water. The Journal of Chemical Physics **79:**926-935.
104. **Salomon-Ferrer R, Götz AW, Poole D, Le Grand S, Walker RC.** 2013. Routine Microsecond Molecular Dynamics Simulations with AMBER on GPUs. 2. Explicit Solvent Particle Mesh Ewald. J Chem Theory Comput **9:**3878-3888.
105. **Tan C, Tan Y-H, Luo R.** 2007. Implicit Nonpolar Solvent Models. The Journal of Physical Chemistry B **111:**12263-12274.
106. **Gohlke H, Case DA.** 2004. Converging free energy estimates: MM-PB(GB)SA studies on the protein-protein complex Ras-Raf. J Comput Chem **25:**238-250.

107. **Hou T, Wang J, Li Y, Wang W.** 2011. Assessing the performance of the MM/PBSA and MM/GBSA methods. 1. The accuracy of binding free energy calculations based on molecular dynamics simulations. J Chem Inf Model **51:**69-82.
108. **Katoh K, Standley DM.** 2013. MAFFT multiple sequence alignment software version 7: improvements in performance and usability. Molecular biology and evolution **30:**772-780.
109. **Waterhouse AM, Procter JB, Martin DM, Clamp M, Barton GJ.** 2009. Jalview Version 2--a multiple sequence alignment editor and analysis workbench. Bioinformatics **25:**1189-1191.

FIGURE LEGENDS

FIG 1 Infection of human and non-human cells by HIV-1, SIVcpzPtt, or SIVcpzPts. (A, D) HIV-1 reporter viruses were used to infect CRFK, FRhL-2, OMK, CV-1, HeLa, and HOS cells using increasing amounts of virus-containing cell supernatant. Firefly luciferase was measured two days later. (B, E) SIVcpzPtt and (C, F) SIVcpzPts reporter viruses were used to infect CRFK, FRhL-2, OMK, CV-1, HeLa, and HOS cells with increasing amounts of virus-containing cell supernatant. Two days post-infection the activity of nanoluciferase was measured. Values are means with standard deviation. Each experiment was performed at least three times and in triplicates. (G) Expression of HIV-1 host factors in HOS and HeLa cells. Immunoblot of cell lysates of HOS and HeLa cells. Tubulin, NUP358, NUP153, CPSF6, TRIM5alpha, CYPA were detected with their specific antibodies, α anti.

FIG 2 Alignment of CA protein sequences of HIV-1, SIVcpzPts, and SIVcpzPtt and residues engaged in interactions with PF74, CYPA, or CPSF6. (A) HIV-1 CA sequence (XXX: Carsten, provide identifier to make it consistent with panel B?) with position weight matrix represented as Weblogo. The HIV-1 CA sequence was taken from the pMDLg/pRRE plasmid. The Weblogo was generated from randomly selected HIV-1 M sequences of different subgroups using MAFFT (108) and JalView (109) (see also Fig. S1). Residues interacting with a ligand are marked with a star; all residues that interact with PF74 also interact with CPSF6 (orange stars), residues only interacting with CPSF6 are marked with red stars, and residues interacting with CYPA are marked with blue stars. (B) SIVcpz CA sequences (JN835461, AF447763) with position weight matrix represented as Weblogo. The randomly picked SIVcpz CA sequences were retrieved from the Los Alamos HIV and SIV sequence database. The Weblogo was generated from HIV sequences using MAFFT (108) and JalView (109) (see

also Fig. S2). Residues interacting with a ligand are marked with a star; all residues that interact with PF74 also interact with CPSF6 (orange stars), residues only interacting with CPSF6 are marked with red stars, and residues interacting with CYPA are marked with blue stars. HIV-1 vs. SIVcpzPts: Identity 78.63%, similarity 87.18%. HIV-1 vs. SIVpzPtt: Identity 89.61%, similarity 94.81%. SIVcpzPts vs. SIVpzPtt: Identity 78.63%, similarity 87.18%. (B – E) Quality assessment of homology models on a per-residue level by TopScore (73) . Blue: TopScore = 0.1 (high structural quality), red: TopScore = 0.8 (low structural quality). (B) Homology model of SIVcpzPts CA monomer based on the structures of the HIV-1 CA crystallized with CPSF6 used as templates. (C) Homology model of SIVcpzPts CA monomer based on the structures of the HIV-1 CA crystallized with PF74 used as templates. (D) Homology model of SIVcpzPtt CA monomer based on the structures of the HIV-1 CA crystallized with CPSF6 used as templates. (E) Homology model of SIVcpzPtt CA monomer based on the structures of the HIV-1 CA crystallized with PF74 used as templates.

FIG 3 Structural models of binding of human CYPA to HIV-1, SIVcpzPts, and SIVcpzPtt CA proteins. (A, B) For SIVcpzPts and SIVcpzPtt, CYPA coordinates were taken after superimposing the proteins to HIV-1 CA bound to CYPA (PDB-ID: 5FJB). Monomers are colored differently; the region in the black box in (A) is shown as a blow-up in (B); side chains of interacting residues are shown as sticks. The interacting residues differ in three positions between HIV-1 CA and SIVcpzPts CA: ILE91 vs. GLN91; ALA92 vs. GLN92; PRO93 vs. ALA93. The interacting residues differ in one position between HIV-1 CA and SIVcpzPtt CA (ALA92 vs. PRO92).

FIG 4 SIVcpz interact with CYPA. (A) HIV-1, SIVcpzPtt, and SIVcpzPts encapsidate CYPA. Viruses were generated by transfection of expression plasmids in HEK293T cells in the absence (-) or presence (+) of 2.5 µM CsA. SIVcpzPtt and SIVcpzPts wild-type (WT) and Luc reporter viruses were analyzed. Protein lysates of purified virions and HEK293T producer cells were subjected to immunoblotting. p24 (capsid) and CYPA were detected with specific antibodies. α anti, Luc luciferase. (B) HIV-1, SIVcpzPtt, and SIVcpzPts GAG interacts with CYPA. HEK293T cells were cotransfected with HIV-1 or SIVcpzPtt or SIVcpzPts and CYPA-GST in the presence (+) or absence (-) of 5 or 10 µM CsA. 48 h later, cells and virions were lysed and the lysate was used for pulldown experiments using GST-sepharose beads. Proteins of cells were subjected to immunoblotting. p24 (capsid) and CYPA were detected with specific antibodies. α anti. (C) G89V in CYPA binding loop of HIV-1, SIVcpzPtt, and SIVcpzPts capsid is important for interaction with CYPA. Similar as in (B) CYPA-GST pulldown of WT and G89V mutated viruses.

FIG 5 Infection of cells by HIV-1 or SIVcpz viruses in the presence of increasing amounts of CsA. HOS, HeLa or FRhL-2 cells were treated with DMSO or CsA (1, 5 or 10 µM) two hours before infection. (A) Infection by HIV-1 luciferase reporter virus. (B) Infection by SIVcpzPtt luciferase reporter virus. (C) Infection by SIVcpzPts luciferase reporter virus. Luciferase activity was measured two days post-infection. Results were normalized to DMSO control. Means and SD (error bars) are shown, Mann Whitney U test was performed. Each experiment was performed three times in triplicates. ns = not significant, * = $p < 0.05$, ** = $p < 0.01$, *** = $p < 0.001$.

FIG 6 Infection of CYPA knockout cells by HIV-1, SIVcpzPtt, or SIVcpzPts. (A) Immunoblot of protein lysates of HOS cell clones with a CYPA knockout (KO). CYPA and tubulin were detected using specific antibodies. α anti. (B) Immunoblot for CYPA knockdown (KD) in HeLa cells (cell population). (C-E) Infection of HOS cell clones 1, 3, 5, and HOS carrying empty vector with either luciferase reporter viruses of (C) HIV-1, (D) SIVcpzPtt, or (E) SIVcpzPts in the absence (DMSO, control) or presence of 5 µM CsA. Luciferase activity was measured two days post-infection. (F-H) Infection of HeLa cells carrying empty vector and CYPA knockdown HeLa cells with (F) HIV-1, (G) SIVcpzPtt or (H) SIVcpzPts in the absence (DMSO, control) or presence of 5 µM CsA. Results were normalized to DMSO control in empty vector cells. Means and SD (error bars) are shown, Mann Whitney U test was performed. Each experiment was performed three times in triplicates. ns = not significant, * = $p < 0.05$, ** = $p < 0.01$, *** = $p < 0.001$.

FIG 7 Infection of cells expressing CPSF6-358 by HIV-1, SIVcpzPtt, or SIVcpzPts. (A) Immunoblot of protein lysates of HOS cells for CPSF6-358 expression. HOS WT (vector, pLNCX2), HOS.CPSF6-358, HOS.CYPA KO.CPSF6-358 (clones 1, 3, 5). HA-tagged CPSF6-358 and GAPDH were detected using their specific antibodies. α anti. Luciferase reporter viruses of (B) HIV-1, (C) HIV-1 A77V capsid mutant, (D) HIV-1 N74D capsid mutant, (E) SIVcpzPtt, (F) SIVcpzPts were used to infect HOS cells with empty vector, HOS cells expressing CPSF6-358, CYPA KO HOS or CYPA KO HOS cells expressing CPSF6-358. Luciferase activity was measured two days post-infection. Results were normalized to infection in empty vector cells. Means and SD (error bars) are shown, Mann Whitney U test was performed. Each experiment was performed three times in triplicates. ns = not significant, * = $p < 0.05$, ** = $p < 0.01$, *** = $p < 0.001$.

FIG 8 Binding of the CPSF6 fragment to CA hexamers. (A) Binding modes of human CPSF6 to homology models of HIV-1 CA and SIVcpzPts/Ptt CA; for the latter two, CPSF6 coordinates were taken after superimposing the proteins to HIV-1 CA bound to CPSF6 (PDB-ID: 4WYM). Monomers are colored differently; the region in the black box is shown as a blow-up in (B); side chains of interacting residues are shown as sticks; residues marked with dashed labels belong to a different chain. (B) The binding pockets differ in three residues between HIV-1 CA and SIVcpzPts CA: SER102 vs. ALA102; LEU172' vs. ILE175'; ASN183' vs. THR186'. The binding pockets differ in one residue between HIV-1 CA and SIVcpzPtt CA: SER178' vs. THR178'. Helix 179'-195' is not shown. The regions in the black boxes in (B) are shown as blow-ups in (C, D, and E); side chains of interacting residues and the CPSF6 fragment are shown as sticks. Numbers indicate distances in Å.

FIG 9 Infection of HOS, HeLa, or FRhL-2 cells with HIV-1, SIVcpzPtt, or SIVcpzPts in the presence of capsid inhibitors PF57 or PF74. (A) Chemical structures of PF74 and PF57. Cells were incubated with increasing amounts of capsid inhibitors (PF57 or PF74) or DMSO for control infections. Two hours later cells were infected with luciferase reporter viruses (B, C) HIV-1, (D, E) SIVcpzPtt, (F, G) SIVcpzPts and luciferase activity was measured two days post-infection. Differences between control and PF74 or PF57 treatment are significant for HIV-1 in all cells ($p<0.05$). For SIVcpzPts differences are significant in HOS cells, but not in HeLa nor FRhL-2 cells, exceptions are marked with * for significant ($p<0.05$). For SIVcpzPtt inhibition is significant in HeLa and Hos cells. The infectivity of SIVcpzPts is significantly reduced only in HOS cells. Means and SD (error bars) are shown, Mann Whitney U test was performed. Each

1118 experiment was performed at least three times in triplicates. ns = not significant * = p < 0.05,
1119 ** = p < 0.01, *** = p < 0.001.

1120

1121 **FIG 10 Infection of CRFK cells with HIV-1, SIVcpzPtt, or SIVcpzPts in the presence of capsid**
1122 **inhibitors PF57 or PF74 and test of antiviral activity of GS-CA1.** (A - C) CRFK cells were
1123 incubated with capsid inhibitors (PF57 or PF74) or DMSO for control infections. Two hours
1124 later cells were infected with luciferase reporter viruses of (A) HIV-1, (B) SIVcpzPtt, (C)
1125 SIVcpzPts and luciferase activity was measured two days post-infection. Means and SD (error
1126 bars) are shown, Mann Whitney U test was performed for significance. (D) Chemical
1127 structure of GS-CA1. (E – G) CRFK, HeLa, HOS, and FRhL2 cells were incubated with capsid
1128 inhibitor GS-CA1 or DMSO. Two hours later cells were infected with luciferase reporter
1129 viruses of (E) HIV-1, (F) SIVcpzPtt, (G) SIVcpzPts and luciferase activity was measured two
1130 days post-infection. Each experiment was performed more than three times in triplicates. ns
1131 = not significant * = p < 0.05, ** = p < 0.01, *** = p < 0.001.

1132

1133 **FIG 11 Infection of human PBMCs and macrophages with HIV-1, SIVcpzPtt, or SIVcpzPts in**
1134 **the presence of capsid inhibitor PF74.** (A, B) PBMCs and (C, D) macrophages were incubated
1135 with PF74 or DMSO and infected with luciferase reporter viruses of HIV-1, SIVcpzPtt,
1136 SIVcpzPts. Luciferase activity was measured two days post-infection. Means and SD (error
1137 bars) are shown, Mann Whitney U test was performed for significance. Each experiment was
1138 performed more than three times in triplicates. ns = not significant * = p < 0.05, ** = p <
1139 0.01, *** = p < 0.001.

1140

FIG 12 Binding of PF74 to CA hexamers. (A, B) Binding modes of PF74 to homology models of HIV-1 CA and SIVcpzPts/Ptt CA proteins; for the latter two, PF74 coordinates were taken after superimposing the proteins to HIV-1 CA bound to PF74 (PDB-ID: 4XFZ). Monomers are colored differently; the region in the black box in (A) is shown as a blow-up in (B); side chains of interacting residues are shown as sticks; residues marked with dashed labels belong to a different chain. The binding pockets differ in one residue between HIV-1 CA and SIVcpzPts CA: LEU172' vs. ILE175'. The binding pockets of HIV-1 CA and SIVcpzPtt CA do not differ. Helix 179'-195' is not shown in (B). (C) Effective binding energies computed by the molecular mechanics Poisson-Boltzmann surface area (MM-PBSA). Effective binding energies of PF74 binding to HIV-1 (blue), SIVcpzPts (pink), and SIVcpzPtt (yellow) CA proteins as a function of the simulation time (left). Values per trajectory are separated by black vertical lines; gray lines separate values computed for each binding site of a CA hexamer. On the right, probability functions of the effective energies across all frames are shown. The average of the effective binding energy for each isoform is marked at the right axis. The standard error of the mean (eq. 1) is < 0.015 kcal mol-1 in all cases.

FIG 13 Infection of HeLa cells in the presence of CsA or infection with CYPA loop mutants (G89V) in the presence of capsid inhibitors. (A – C) HeLa cells were incubated with 1, 4 or 8 µM capsid inhibitor PF74 or DMSO or capsid inhibitor together with CsA (1 or 10 µM). Two hours later cells were infected with luciferase reporter viruses (A) HIV-1, (B) SIVcpzPtt, or (C) SIVcpzPts and luciferase activity was measured two days post-infection. Results were normalized to infection of cells treated with DMSO (control) or CsA only treated cells. (D –I) Infection of HeLa cells with CYPA loop mutants (G89V) of HIV-1, SIVcpzPtt, or SIVcpzPts in the presence of capsid inhibitors. Cells were incubated with increasing amounts of capsid

inhibitor (D - F) PF74 or (G –I) GS-CA1 or DMSO for control infections. Two hours later cells were infected with luciferase reporter viruses (D, G) HIV-1 and HIV-1 G89V, (E, H) SIVcpzPtt and SIVcpzPtt G89V, (F, I) SIVcpzPts and SIVcpzPts G89V. Luciferase activity was measured two days post-infection. Results were normalized to infection of cells treated with DMSO. Each experiment was performed three times in triplicates.

FIG 14 Infection of CYPA-KO cells with HIV-1, SIVcpzPtt, or SIVcpzPts in the presence of capsid inhibitors. HOS.CYPA KO and HeLa.CYPA KD cells were incubated with increasing amounts of capsid inhibitors (PF57 or PF74) or DMSO for control infections. Two hours later cells were infected with luciferase reporter viruses (A to D) HIV-1, (E to H) SIVcpzPtt, (I to L) SIVcpzPts and luciferase activity was measured two days post infection. Results were normalized to infection of cells treated with DMSO. Each experiment was performed three times in triplicates.

Table 1: Homology modelling: Used templates, sequence identities and similarities, and TopScore assessment

PF74:

Model	Templates	Sequence identity[a]	Sequence similarity[a]	TopScore[b]	TopScore Single[b]
HIV1_PF74	4XFZ_A, 4QNB_A, 4XRO_A, 4U0E_A, 6AXV_A	92.2, 92.2, 88.7, 89.6, 91.8	92.2, 92.2, 89.6, 89.6, 92.2	0.17	0.17
SIVcpzPts_PF74	4XFZ_A, 4QNB_A, 4XRO_A, 4U0E_A, 6AXV_A	74.8, 73.1, 71.0, 71.0, 74.6	81.2, 80.8, 78.6, 78.2, 81.6	0.19	0.20
SIVcpzPtt_PF74	4XFZ_A, 4QNB_A, 4XRO_A, 4U0E_A, 6AXV_A	83.1, 82.7, 80.5, 80.5, 82.7	87.9, 87.9, 85.7, 85.3, 87.9	0.17	0.15

CPSF6:

Model	Templates	Sequence identity[a]	Sequence similarity[a]	TopScore	TopScore Single
HIV1_CPSF6	4WYM_A, 4U0A_A, 6AY9_A, 4B4N_A	90.9, 88.3, 94.4, 58.9	90.9, 88.3, 94.4, 58.9	0.19	0.17
SIVcpzPts_CPSF6	4WYM_A, 4U0A_A, 6AY9_A, 4B4N_A	63.3, 70.1, 75.2, 44.9	70.5, 77.4, 81.6, 51.3	0.21	0.20
SIVcpzPtt_CPSF6	4WYM_A, 4U0A_A, 6AY9_A, 4B4N_A	82.3, 79.7, 84.9, 52.0	86.6, 84.0, 89.6, 55.4	0.18	0.16

Cyclophilin A:

Model	Templates	Sequence identity [a]	Sequence similarity [a]	TopScore	TopScore Single
HIV1_CYPA	5FJB_A, 1FGL_B, 1M9D_C	92.6, 4.3, 60.2	94.0, 4.3, 60.6	0.31	0.23
SIVcpzPts_CYPA	5FJB_A, 1FGL_B, 1M9D_C	74.0, 2.1, 46.1	81.6, 2.6, 52.1	0.33	0.28
SIVcpzPtt_CYPA	5FJB_A, 1FGL_B, 1M9D_C	84.0, 3.5, 55.0	89.6, 3.9, 58.4	0.31	0.23
Cyclophilin A	5FJB_C, 1FGL_A, 1M9D_B	99.4, 100.0, 98.8	99.4, 100.0, 98.8	0.09	0.17

[a] In %.

[b] Lower TopScore or TopScore Single values indicate better structural quality. The values are bounded between [0, 1].

Fig. 1

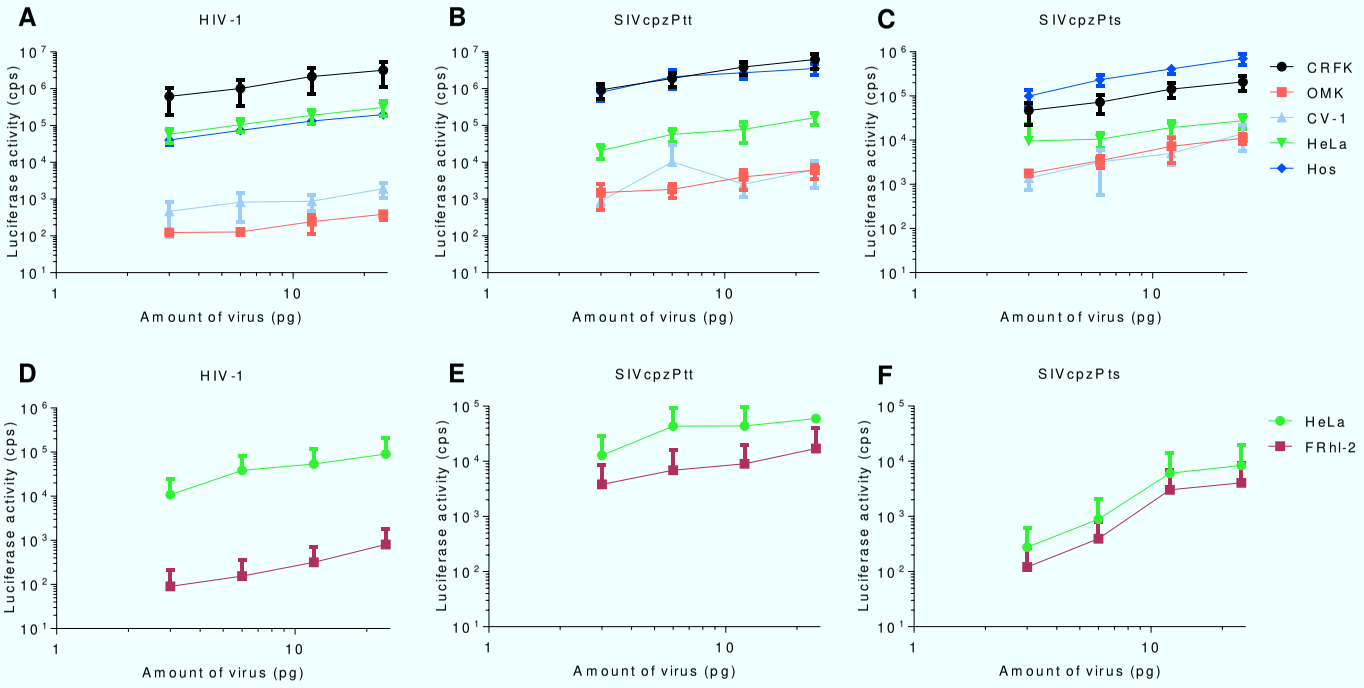
A
HIV-1
B
SIVcpzPtt
C
SIVcpzPts
D
HIV-1
E
SIVcpzPtt
F
SIVcpzPts
Luciferase activity (cps)
Amount of virus (pg)
CRFK
OMK
CV-1
HeLa
Hos
HeLa
FRhl-2

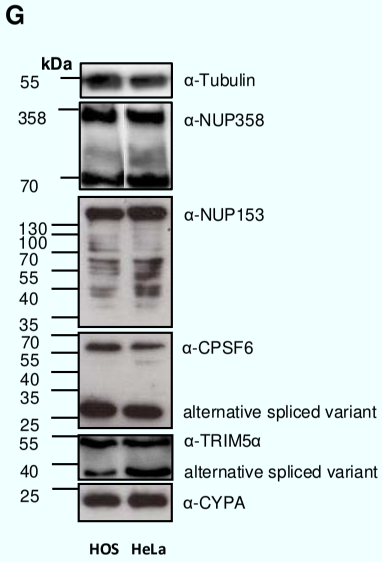
G
kDa
55
358
70
130
100
70
55
40
35
70
55
40
35
25
55
40
25
α-Tubulin
α-NUP358
α-NUP153
α-CPSF6
alternative spliced variant
α-TRIM5α
alternative spliced variant
α-CYPA
HOS
HeLa

Fig. 2

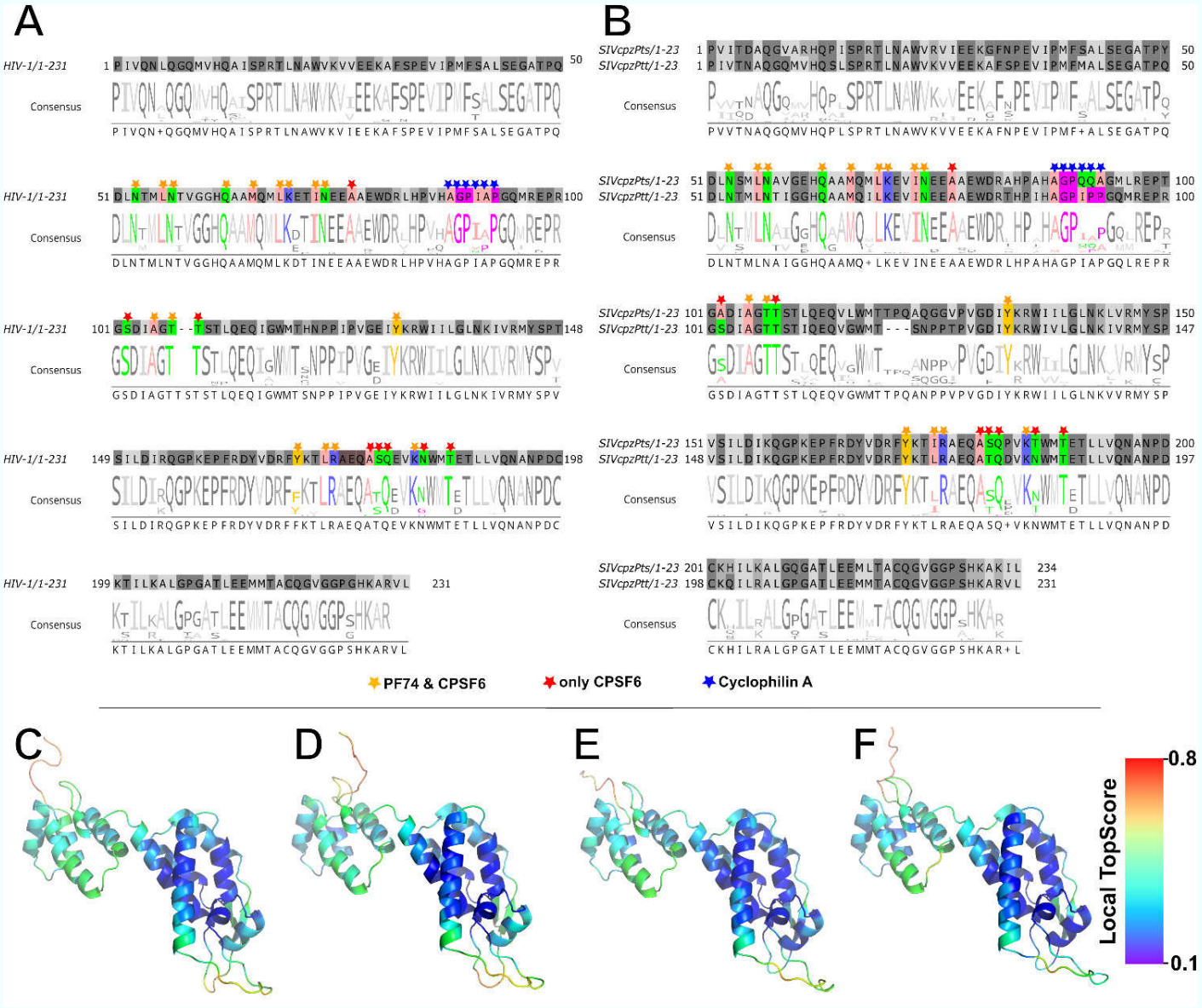
A
B
HIV-1/1-231
Consensus
SIVcpzPts/1-23
SIVcpzPtt/1-23
PF74 & CPSF6
only CPSF6
Cyclophilin A
C
D
E
F
Local TopScore
0.8
0.1

Fig. 3

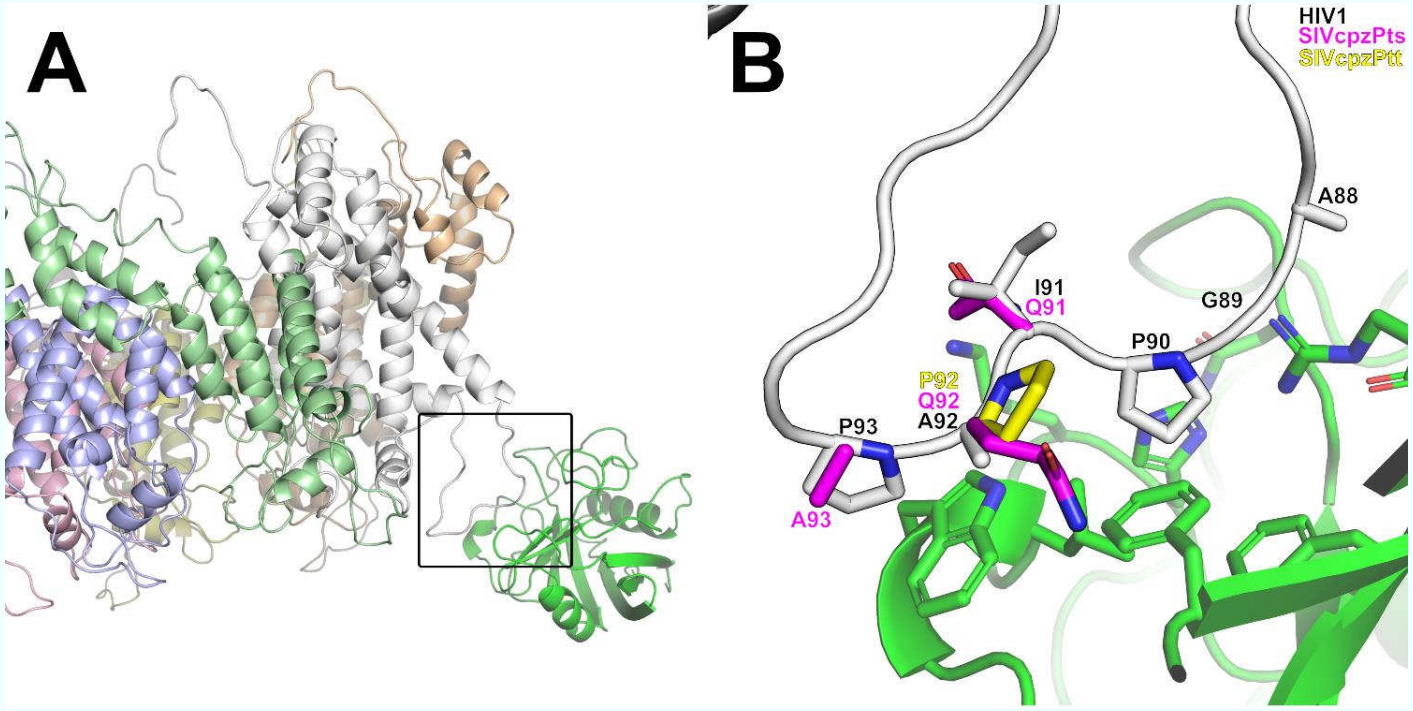
A
B
HIV1
SIVcpzPts
SIVcpzPtt
A88
I91
Q91
G89
P90
P92
Q92
A92
P93
A93

Fig. 4

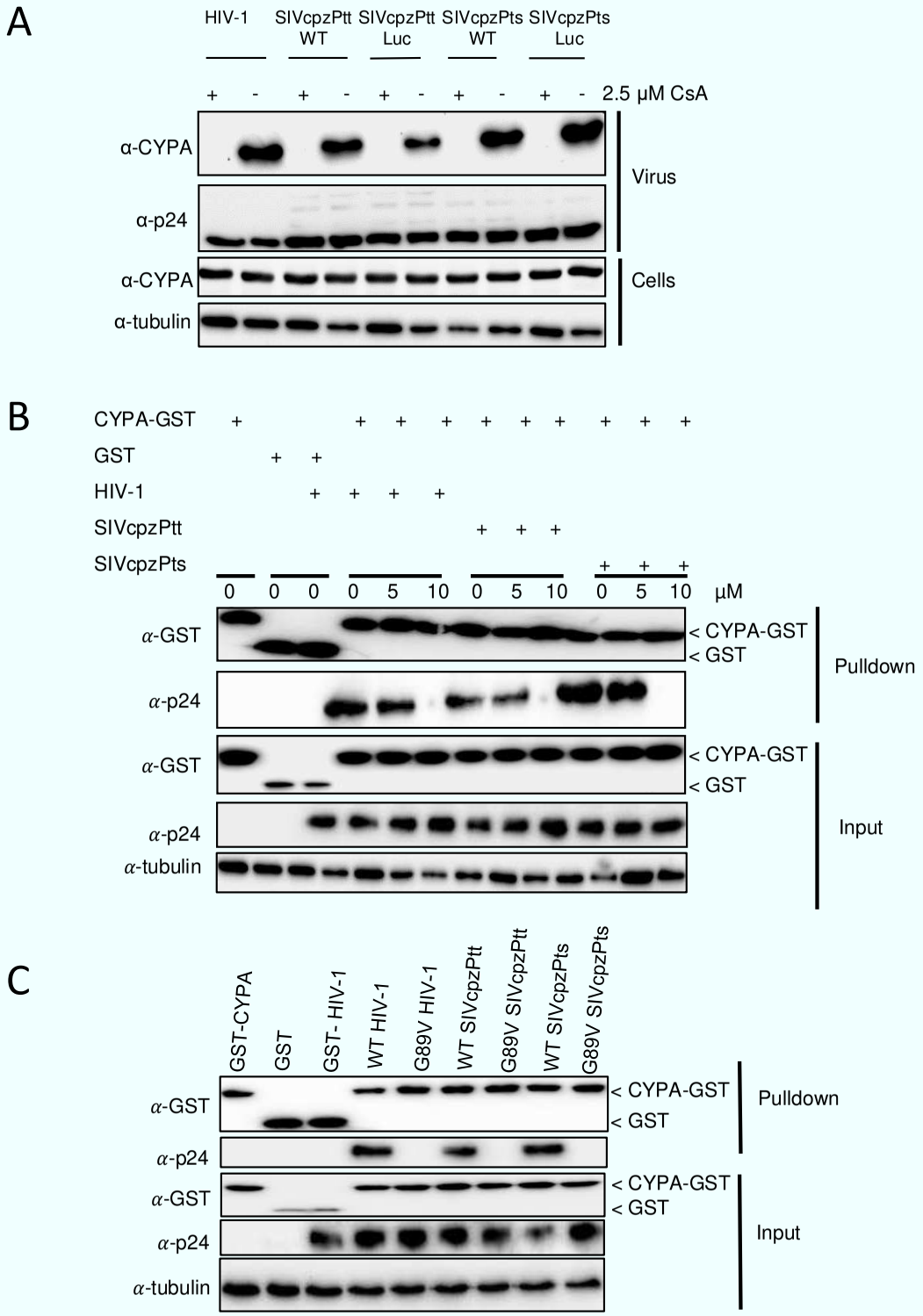
A
HIV-1
SIVcpzPtt WT
SIVcpzPtt Luc
SIVcpzPts WT
SIVcpzPts Luc
+ - + - + - + - + - 2.5 μM CsA
α-CYPA
α-p24
α-CYPA
α-tubulin
Virus
Cells
B
CYPA-GST
GST
HIV-1
SIVcpzPtt
SIVcpzPts
0 0 0 0 5 10 0 5 10 0 5 10 μM
α-GST
α-p24
α-GST
α-p24
α-tubulin
< CYPA-GST
< GST
< CYPA-GST
< GST
Pulldown
Input
C
GST-CYPA
GST
GST- HIV-1
WT HIV-1
G89V HIV-1
WT SIVcpzPtt
G89V SIVcpzPtt
WT SIVcpzPts
G89V SIVcpzPts
α-GST
α-p24
α-GST
α-p24
α-tubulin
< CYPA-GST
< GST
< CYPA-GST
< GST
Pulldown
Input

Fig. 5

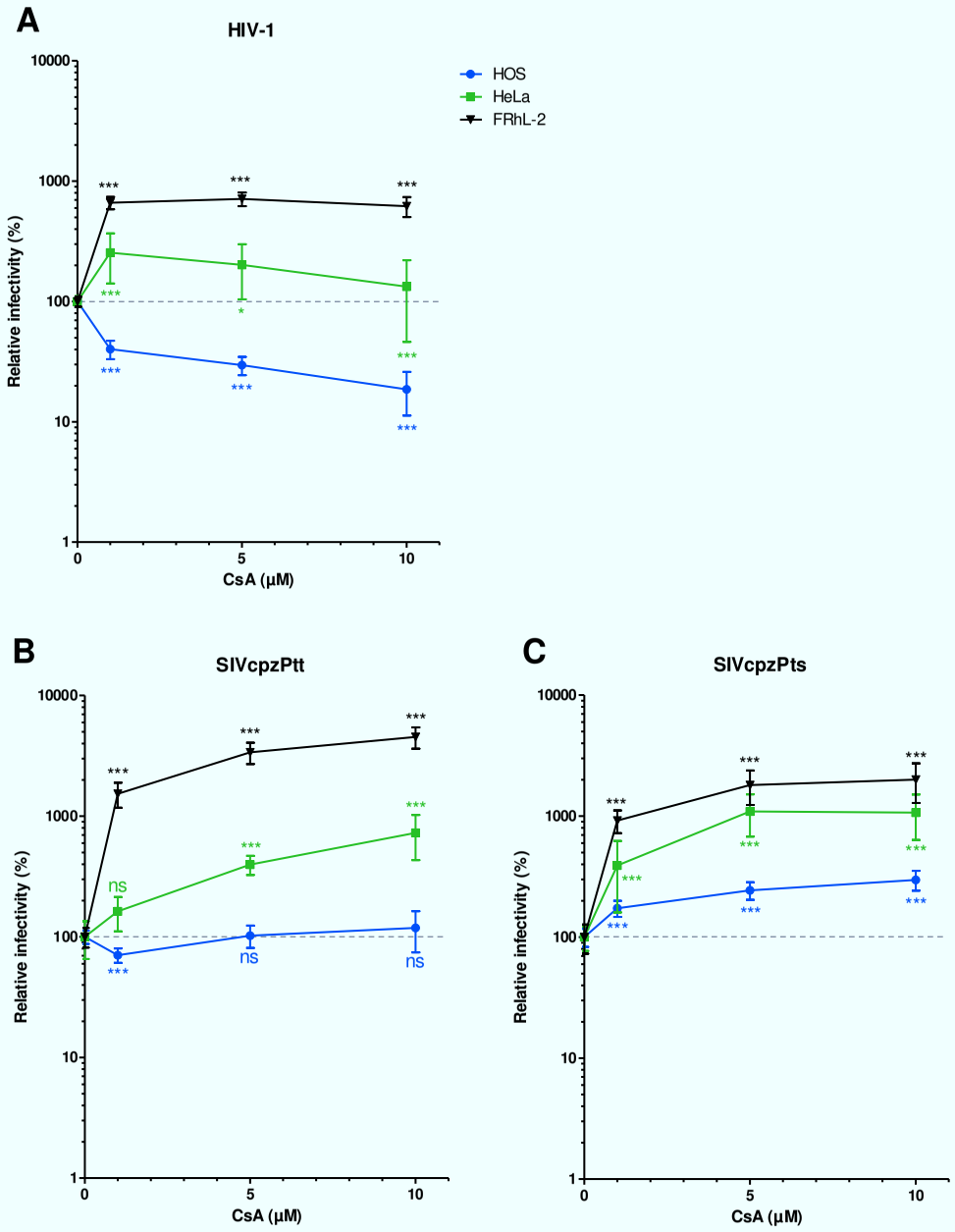
A
HIV-1
HOS
HeLa
FRhL-2
Relative infectivity (%)
CsA (μM)
B
SIVcpzPtt
ns
C
SIVcpzPts

Fig. 6

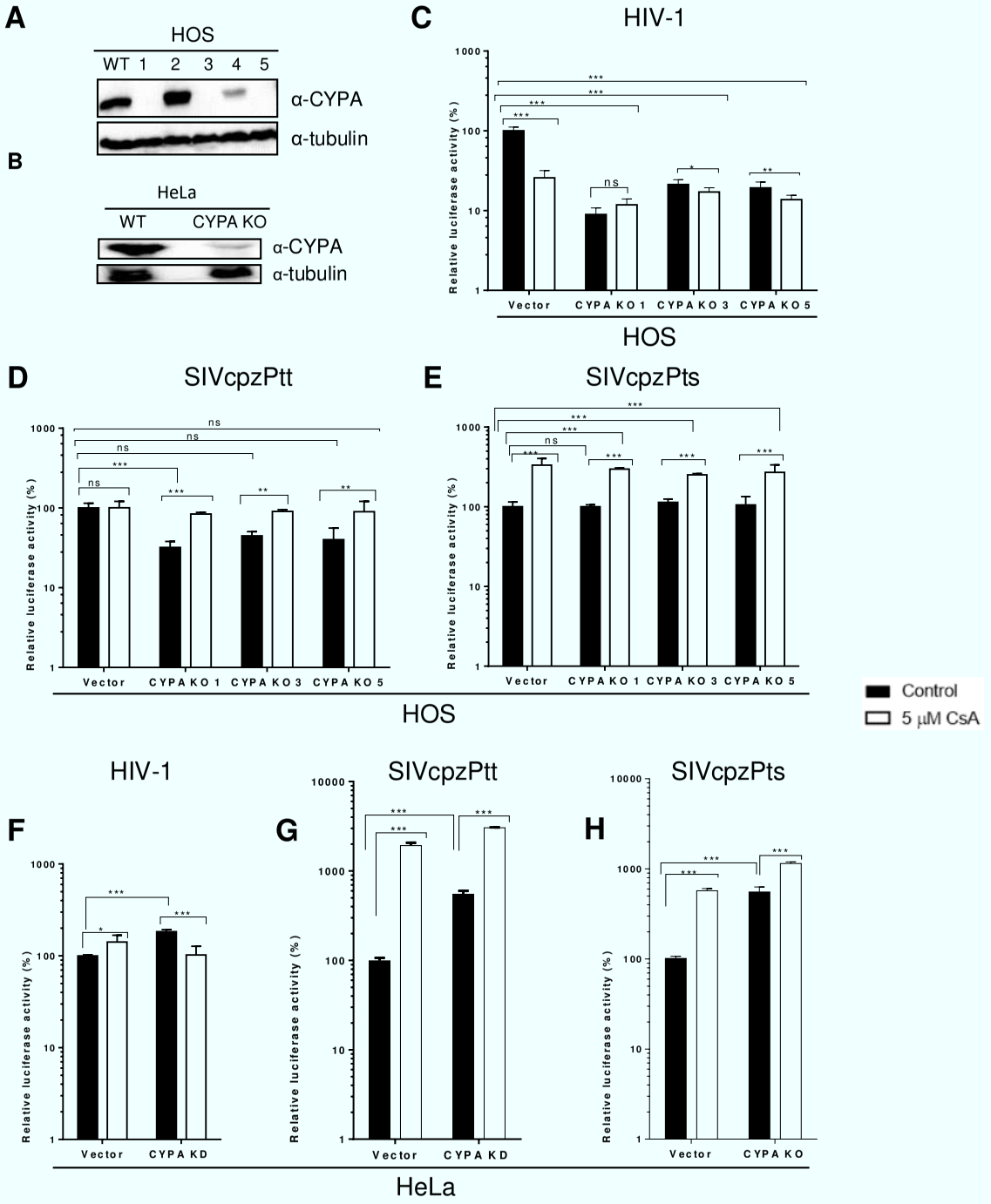
A
HOS
WT 1 2 3 4 5
α-CYPA
α-tubulin
B
HeLa
WT CYPA KO
α-CYPA
α-tubulin
C
HIV-1
Relative luciferase activity (%)
Vector
CYPA KO 1
CYPA KO 3
CYPA KO 5
HOS
D
SIVcpzPtt
E
SIVcpzPts
HOS
Control
5 μM CsA
F
HIV-1
G
SIVcpzPtt
H
SIVcpzPts
CYPA KD
CYPA KO
HeLa

Fig. 7

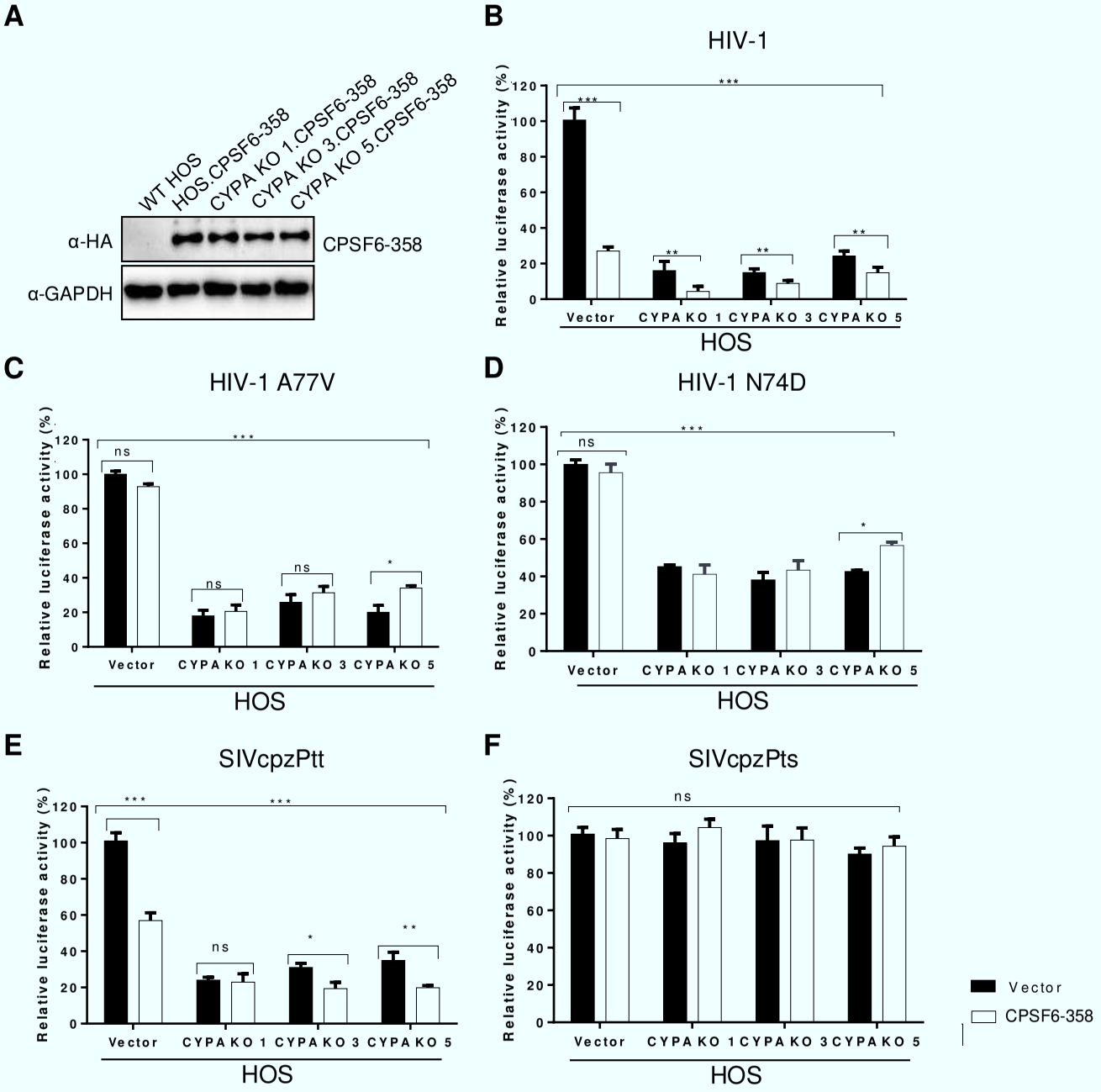
A
WT HOS
HOS.CPSF6-358
CYPA KO 1.CPSF6-358
CYPA KO 3.CPSF6-358
CYPA KO 5.CPSF6-358
α-HA
CPSF6-358
α-GAPDH
B
HIV-1
Relative luciferase activity (%)
Vector
CYPA KO 1
CYPA KO 3
CYPA KO 5
HOS
C
HIV-1 A77V
D
HIV-1 N74D
E
SIVcpzPtt
F
SIVcpzPts
Vector
CPSF6-358

Fig. 8

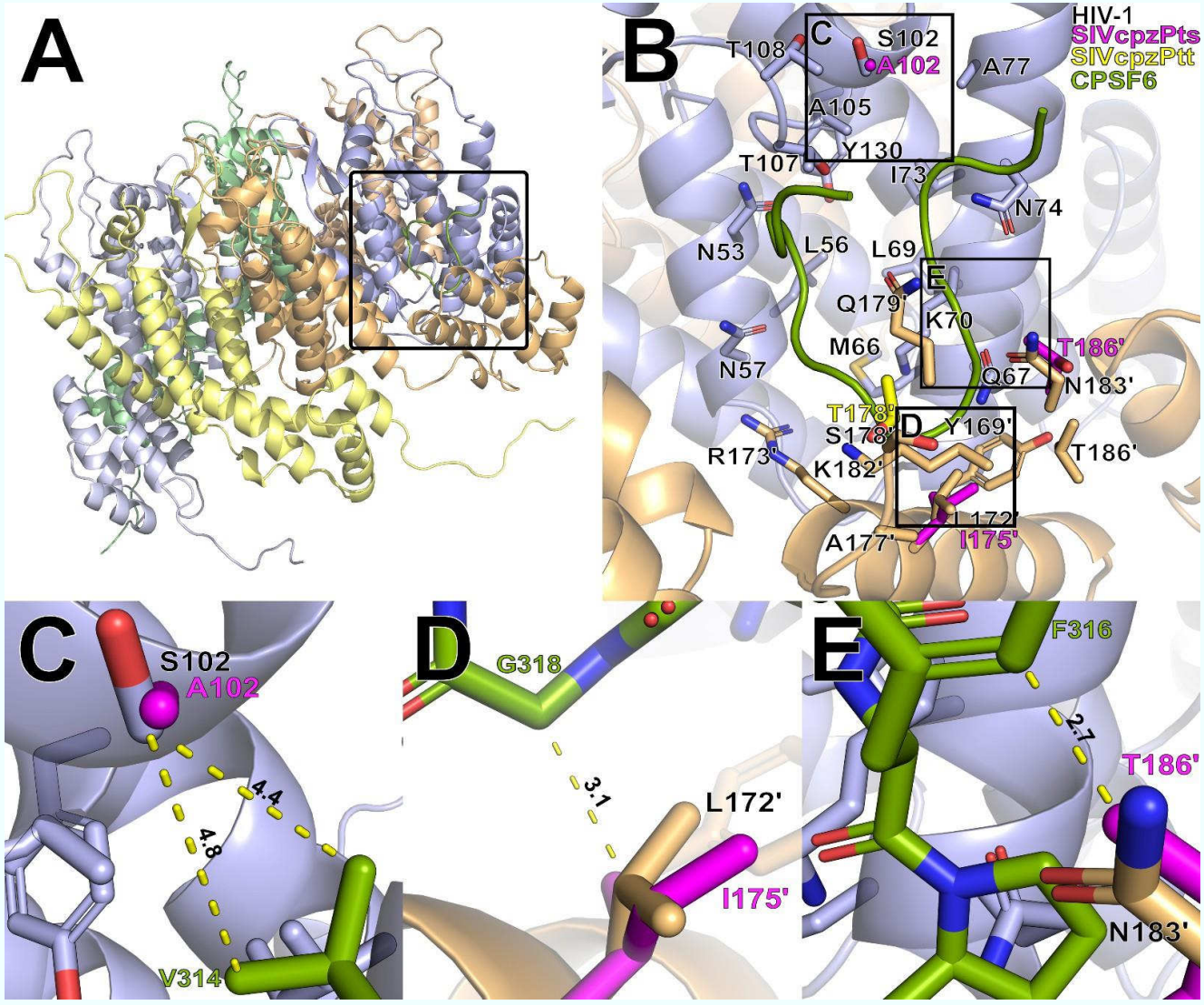
A
B
C
D
E
HIV-1
SIVcpzPts
SIVcpzPtt
CPSF6
T108
S102
A102
A77
A105
Y130
T107
I73
N74
N53
L56
L69
Q179'
K70
M66
T186'
N57
Q67
N183'
T178'
S178'
Y169'
R173'
K182'
T186'
L172'
A177'
I175'
S102
A102
4.4
4.8
V314
G318
3.1
L172'
I175'
F316
2.7
T186'
N183'

Fig. 9

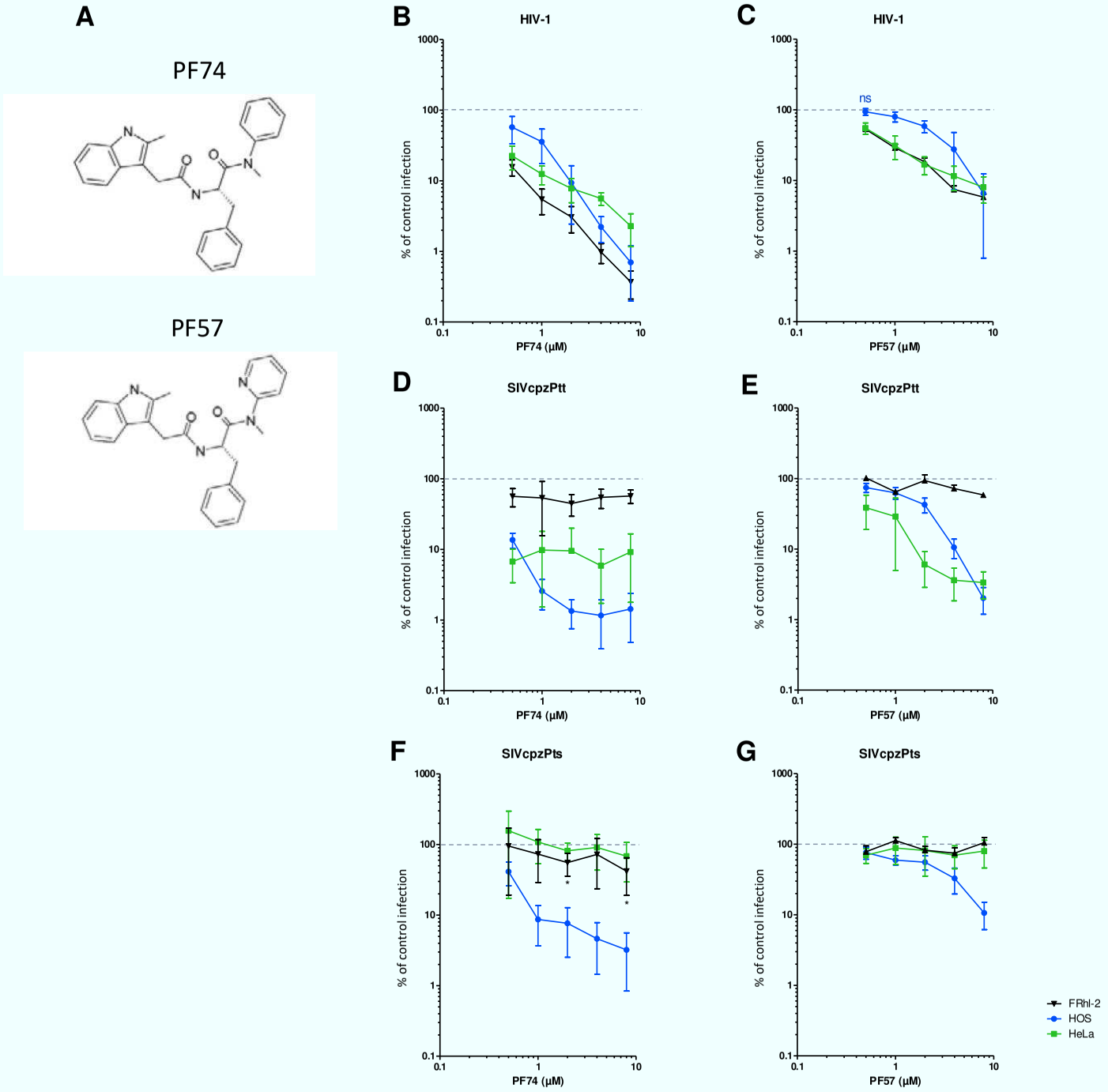
A
PF74
PF57
B
HIV-1
% of control infection
PF74 (μM)
C
HIV-1
ns
% of control infection
PF57 (μM)
D
SIVcpzPtt
% of control infection
PF74 (μM)
E
SIVcpzPtt
% of control infection
PF57 (μM)
F
SIVcpzPts
% of control infection
PF74 (μM)
G
SIVcpzPts
% of control infection
PF57 (μM)
FRhI-2
HOS
HeLa

Fig. 10

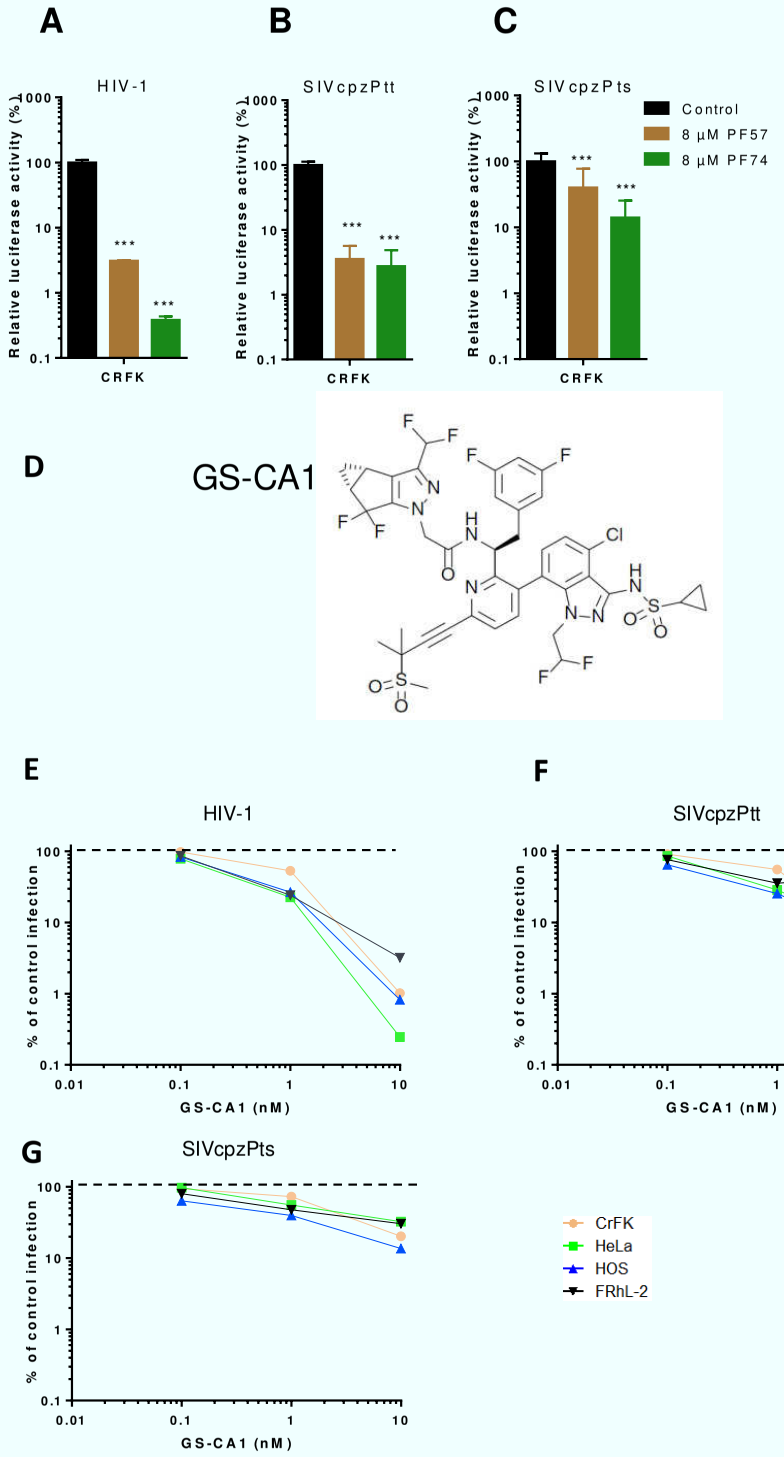
A
B
C
HIV-1
SIVcpzPtt
SIVcpzPts
Relative luciferase activity (%)
CRFK
Control
8 µM PF57
8 µM PF74
***
D
GS-CA1
E
F
G
% of control infection
GS-CA1 (nM)
CrFK
HeLa
HOS
FRhL-2

Fig. 11

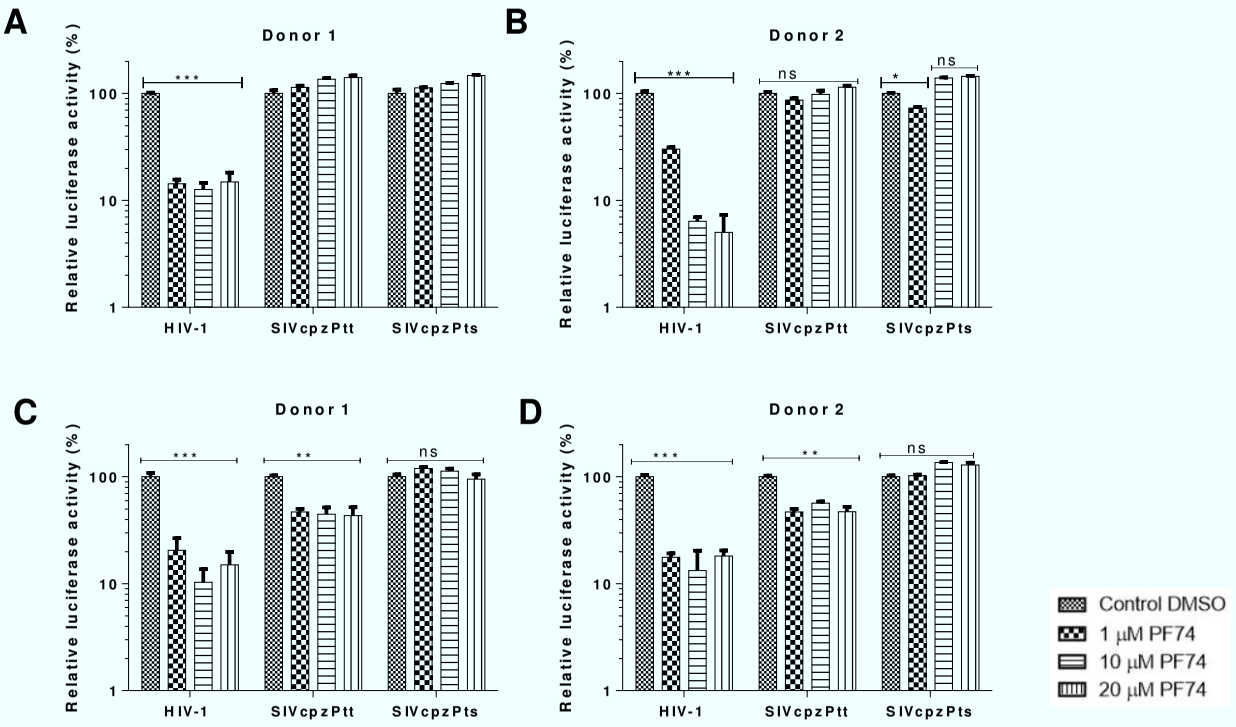
A
Donor 1
Relative luciferase activity (%)
100
10
1
***
HIV-1
SIVcpzPtt
SIVcpzPts
B
Donor 2
Relative luciferase activity (%)
***
ns
*
ns
HIV-1
SIVcpzPtt
SIVcpzPts
C
Donor 1
Relative luciferase activity (%)
***
**
ns
HIV-1
SIVcpzPtt
SIVcpzPts
D
Donor 2
Relative luciferase activity (%)
***
**
ns
HIV-1
SIVcpzPtt
SIVcpzPts
Control DMSO
1 μM PF74
10 μM PF74
20 μM PF74

Fig. 12

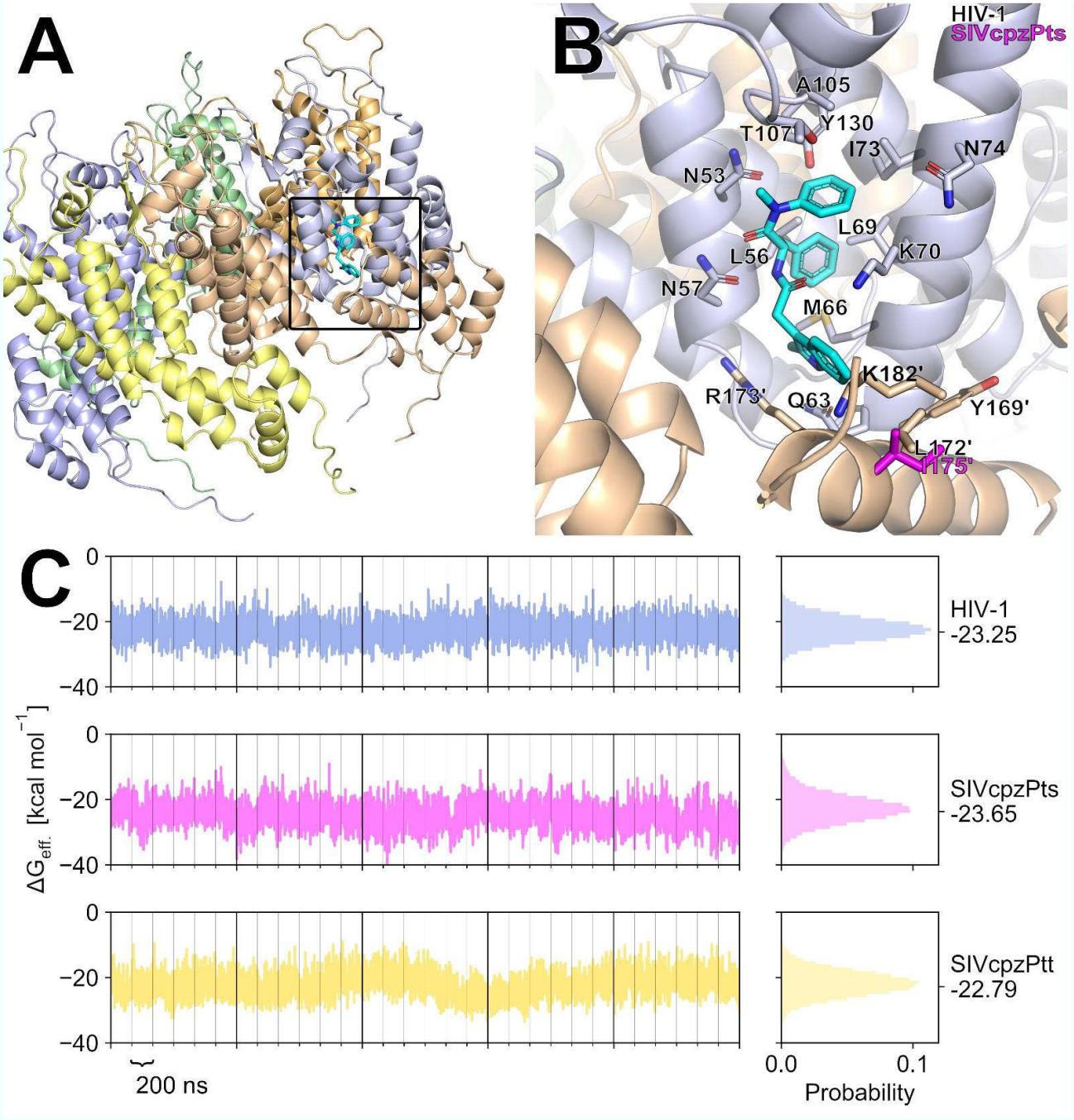
A
B
HIV-1
SIVcpzPts
A105
Y130
T107
I73
N74
N53
L69
L56
K70
N57
M66
K182'
R173'
Q63
Y169'
L172'
I175'
C
0
−20
−40
ΔG_eff. [kcal mol^−1]
HIV-1
-23.25
SIVcpzPts
-23.65
SIVcpzPtt
-22.79
200 ns
0.0
0.1
Probability

Fig. 13

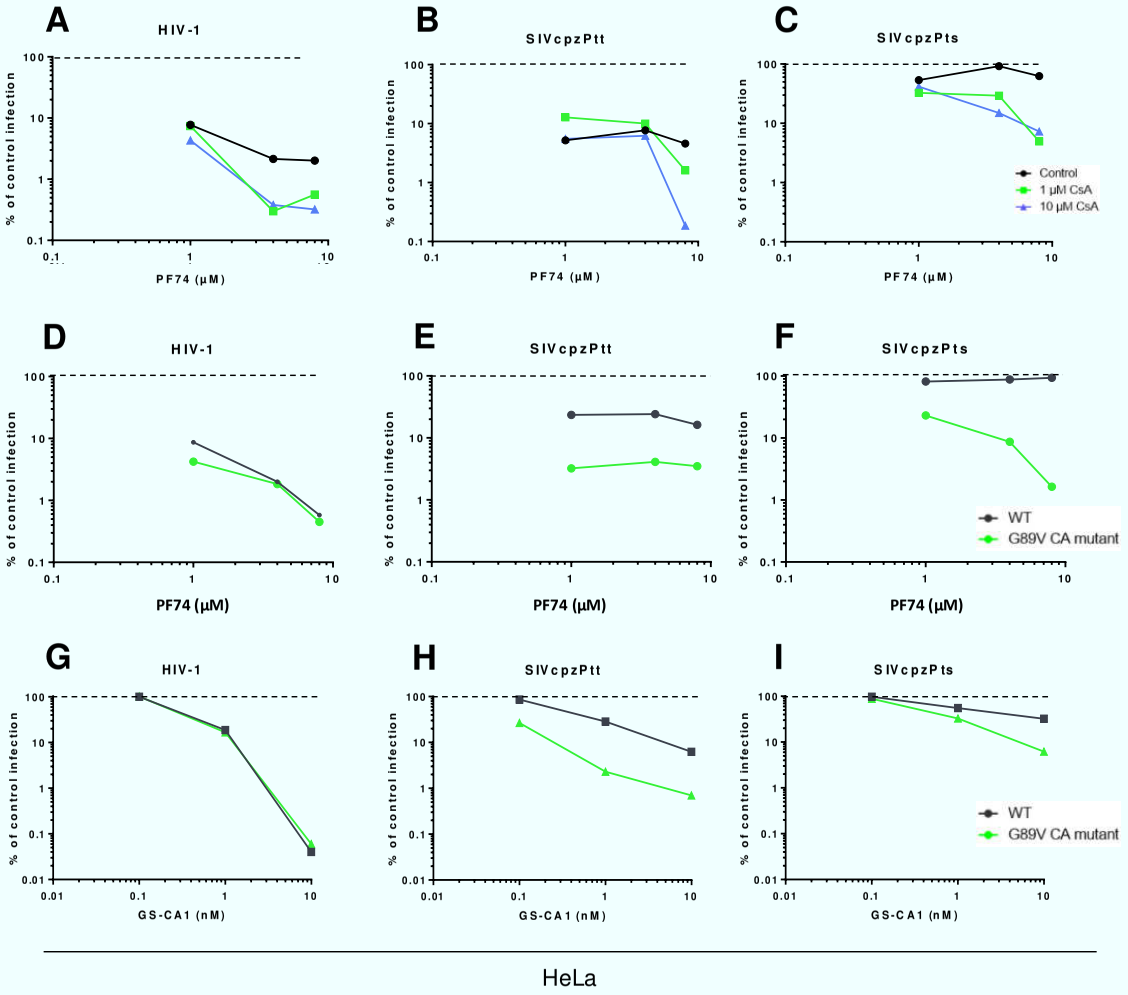
A
HIV-1
B
SIVcpzPtt
C
SIVcpzPts
% of control infection
PF74 (μM)
Control
1 μM CsA
10 μM CsA
D
HIV-1
E
SIVcpzPtt
F
SIVcpzPts
WT
G89V CA mutant
G
HIV-1
H
SIVcpzPtt
I
SIVcpzPts
GS-CA1 (nM)
HeLa

Fig. 14

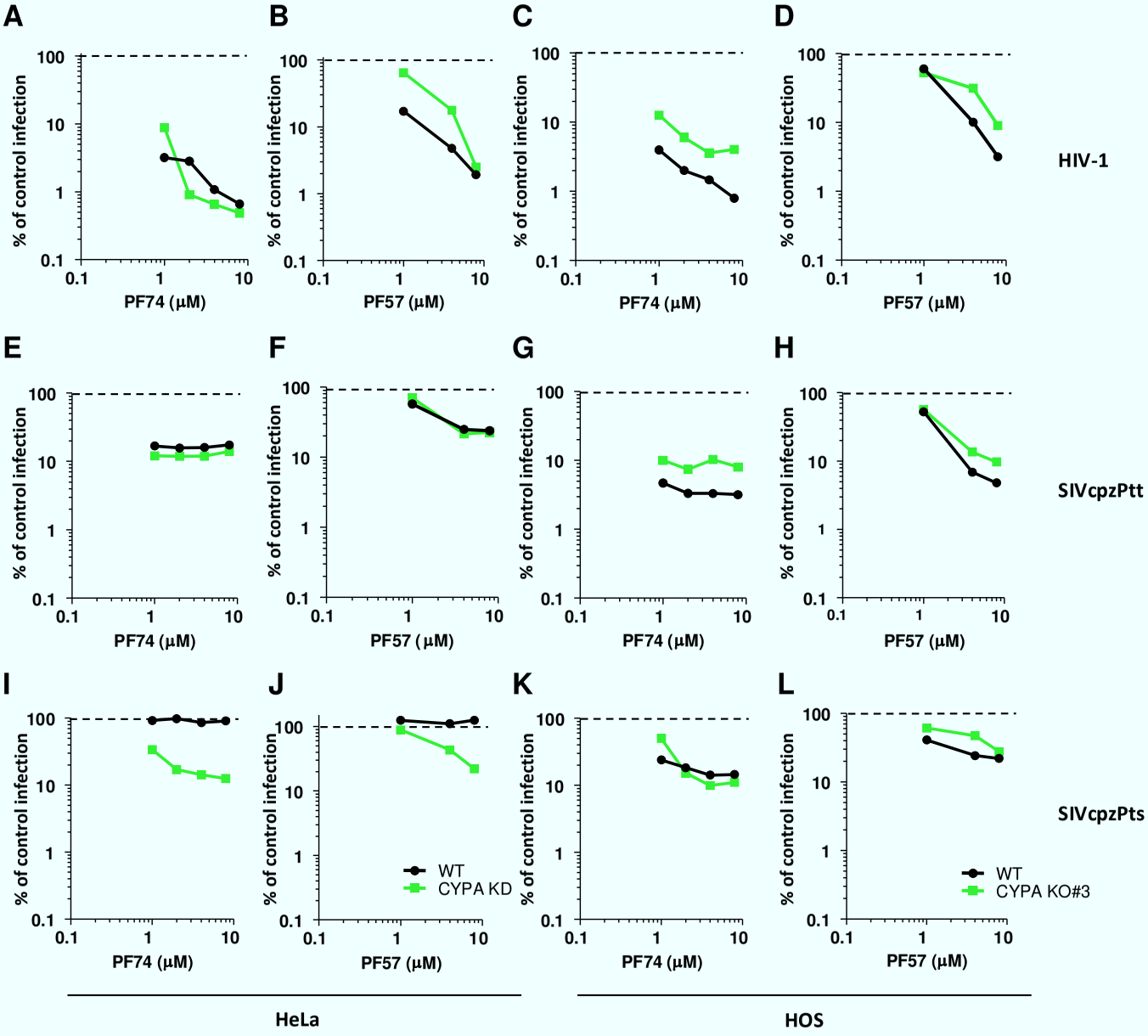
A
B
C
D
E
F
G
H
I
J
K
L
% of control infection
100
10
1
0.1
0.1
1
10
PF74 (μM)
PF57 (μM)
HIV-1
SIVcpzPtt
SIVcpzPts
WT
CYPA KD
CYPA KO#3
HeLa
HOS